MASTER

Design and optimization of a coreless linear actuator with three degrees of freedom

van Essen, J.M.

Award date:
2004

TU/e Eindhoven University of Technology
/Section Electromechanics and Power Electronics

Master of Science Thesis

Design and Optimization of a Coreless Linear Actuator with Three Degrees of Freedom

EPE 2004-11 **J.M. van Essen**

Coaches: **Dr. E. Lomonova, ir. J.W. Jansen**

Eindhoven, November 2004

Abstract

A coreless linear electromechanical actuator with permanent magnets on the moving part and coils on the stationary part has been designed. The actuator includes electromagnetic levitation and has three degrees of freedom (DoF): propulsion (x-direction), suspension (z-direction) and pitch (rotation around the y-axis). This actuator is a pre-prototype for the eventual design of a 6-DoF planar actuator. The advantage of this actuator topology is that the platform (moving part) is entirely contactless. This means that there are no disturbing influences, for instance from cable slabs, present. The 3-DoF actuator is designed in such a way that it is useful for gaining experience that can be used in the design and measurement process of the eventual 6-DoF planar actuator.

Relevant literature is searched for comparable actuators. Only few actuators are comparable, and of those actuators, very little performance indexes are known. Using this limited information, three topology options are created for the 3-DoF actuator. The option that is used has a straight array of coils and a magnet array that is rotated 45 degrees around z-axis with respect to the coils. This design has the most interesting properties for the 6-DoF planar design.

The actuator design is optimized for both maximum acceleration in x- and z-directions and minimum acceleration ripple in those directions, using a parametric search. Constraints are set on this optimization by available magnet sizes and dimensions of the H-drive that will support the pre-prototype. After the optimal design is derived, the coil specifications are adapted to fit the available amplifiers. Next, a thermal analysis of the design is performed and internal parasitic effects are analyzed.

The actuator is built and tested in the laboratory of the EPE group. Measurements demonstrate that the actuator indeed shows the predicted performance. Results of the project are submitted to the IEEE IEMDC 2005 conference for publication.

Preface

This thesis concludes the work I have done on the final project to obtain my Master of Science degree. It describes the period of almost one year that I have worked on this project and is a partial fulfillment of my Master's degree.

I would like to thank ir. Helm Jansen and ir. Nelis van Lierop for their extensive support in both theoretical work and the experiment, dr. Helena Lomonova and prof.dr.ir. André Vandenput for their coaching and motivating me to become an Electromechanical Engineer.

Special thanks to Marijn Uyt De Willigen for building the test-setup and all his technical support. Furthermore, thanks to ir. Korneel Wijnands of Prodrive and ir. Peter van Gils of ASML for supplying the amplifiers.

Furthermore, I would like to thank ir. Peter Krechting PDEng of Tecnotion for his cooperation and advice on manufacturing the coils and placing them on the support, Bakker Magnetics (ing. Maarten de Bekker) for manufacturing the magnet array and the GTD (Gemeenschappelijke Technische Dienst) of the University, in particular Harrie de Laat, for their flexible way of working, their support and useful suggestions to improve the mechanical aspects of the setup.

Finally, I wish to thank all other people that helped me during this project.

Contents

List of symbols

symbol	dimension	used for
ε_0	F/m	permittivity of vacuum
ε_r	-	relative permittivity
μ_0	H/m	permeability of vacuum ($4\pi \cdot 10^{-7}$)
μ_r	-	relative permeability
τ	m	pole pitch
ρ	Ω m	resistivity
σ	T	magnetic surface charge
ψ	Wb	magnetic flux linkage
$\vec{\phi}$	Wb	flux (vector)
A	m^2	area
$a_{x,y,z}$	m/s^2	acceleration
A	Wb/m	magnetic vector potential
B	T	magnetic flux density
B_r	T	magnetic remanence
D	C/m^2	electric flux density
e	-	emissivity
E	V/m	electric field strength
F, f	N	force
H	A/m	magnetic field strength
H	mm	coil height
H_c	W	heat flow
HB	mm	width of the longitudinally magnetized magnets
HM	mm	height of the pole magnets
i,I	A	current
J	A/m^2	current density
k	W/mK	thermal conductivity
l	m	conductor length
L	m	total machine length
m	kg	mass
M	H	mutual inductance
M	A/m	magnetization
n	-	arbitrary number
N	-	number of turns
NA	-	number of power amplifiers
P	W	electric power
P_{rel}	W	relative electric power

Q	J	heat flux
R	Ω	resistance
$\mathbf{u}$	-	unit vector
t	s	time
T	°C	temperature
T_{abs}	K	absolute temperature
$\mathbf{v}$	m/s	speed
V	m^3	volume
$\mathbf{W}$	-	wrench (forces and torque vector)
WM	mm	width of the pole magnets
w_m	J/m^3	magnetic energy density
w'_m	J/m^3	magnetic energy density
W_m	J	total magnetic energy
W'_m	J	total magnetic co-energy

subscript	refers to
m	related to the mover (translator)
n	normal direction
s	related to the stator
t	tangential direction
x	x-direction
y	y-direction
z	z-direction

Acronyms	
FEM	Finite Element Method
NdFeB	Neodymium Ferrite Boron (rare-earth magnetic material)
DoF	Degree of Freedom

Chapter 1
Introduction

1.1 Background and goal

The goal of this thesis is to present the design, electromagnetic optimization and realization of a 3-DoF (Degree of Freedom) linear actuator. Furthermore, measurement results are compared to calculations. This 3-DoF actuator, which is the subject of this Master's thesis, is a step on the way to the design of a 6-DoF planar actuator. The three mechanical DoFs are movement in x-direction (propulsion), movement in z-direction (suspension) and rotation around the y-axis (pitch).

The project is a part of an innovation driven research program (IOP-EMVT, Innovatief Onderzoeks Programma - Elektromagnetische VermogensTechniek), on which two PhD students are working, ir. J.W. Jansen and ir. C.M.M. van Lierop.

1.2 Outline of the actuator

1.2.1 IOP-EMVT planar actuator

The goal of the IOP-EMVT project 02204 A & B "Contactless multi-dimensional actuator technology" is the design, optimization and realization of a moving platform with permanent magnets, suspended and propelled with electromagnetic forces. This actuator should be magnetically levitated and should move in a horizontal plane over relatively long distances (long stroke actuator). The moving part has to be stabilized and accurately controlled in six DoF.

Contactless electromagnetic levitation and propulsion have promising characteristics, such as almost no friction, no unpredictable mechanical disturbances owing to cable slabs and suitability to operate in vacuum conditions. Therefore, the actuator could be interesting for use in future lithographic systems. Figure 1.1 shows an artist's impression of this actuator.

1.2.2 3-DoF linear actuator

As mentioned before, the 3-DoF actuator is a preliminary step for the eventual design of the 6-DoF actuator. An artist's impression of this actuator is shown in figure 1.2. This design has a number of purposes. First, it is meant to prove the principal ideas of contactless magnetic levitation of a platform. Second, it will

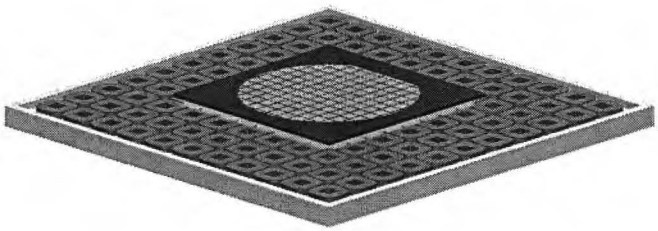

Figure 1.1. *Artist's impression of the 6-DoF actuator*

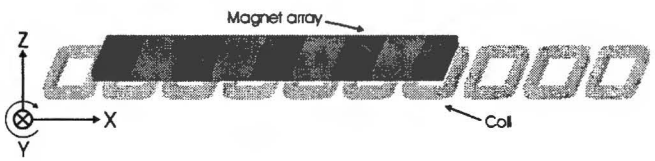

Figure 1.2. *Artist's impression of the 3-DoF actuator*

be used to validate the design and simulation tools. Finally, the actuator will be identified to design and test a 3-DoF controller.

The experiences gained with this 3-DoF actuator can then be used within the project to further design and realize the 6-DoF planar actuator. Because this is the main goal of the 3-DoF actuator, no specifications (such as maximum speed or acceleration) have been defined. The actuator is meant to prove the operating principles and test controller strategies, therefore performance is not an important issue.

1.3 Definitions

The following definitions are used in this thesis:

stroke is the maximum movement length in x direction, or with planar actuators, in x- or y-directions

propulsion is the movement in x-direction

suspension is the movement in z-direction

DoF means Degree of Freedom

Yaw is the rotation around the z-axis

Pitch is the rotation around the y-axis

Roll is the rotation around the x-axis

Translator or mover The moving part of a linear actuator.

Stator The stationary part of a linear actuator.

Pole pitch is the distance between the poles, this means between the north and south poles on the translator.

Halbach array is a type of magnet array, first proposed by K. Halbach, where one or more magnets, magnetized perpendicular to the pole magnets or in the shape of an arc, are placed in between the pole (north/south) magnets. As a result, the magnetic field strength above the array is very low, while the magnetic field strength below the array is up to a factor $\sqrt{2}$ higher [1].

Longitudinally magnetized magnets are the magnets placed in between the pole magnets in the Halbach array.

NdFeB is short for Neodymium Ferrite Boron, which is a rare-earth permanent magnetic material, often used in electrical machines.

1.4 Structure of the thesis

This chapter provides an introduction to the project and the general goal of this work. Chapter 2 gives an overview of existing linear and planar permanent magnet actuators. The initial design and its operating principles are also presented in this chapter.

The electromagnetic theory behind the actuator, as well as the calculation methods are presented in chapter 3. This chapter also describes the software that is used within the project.

Chapter 4 handles about the design process, starting with the electromagnetic optimization of the design and its constraints, and moving via an eddy current analysis and a thermal analysis to the final design.

The realization of the actuator and the details of the experiments with the test setup are described in chapter 5. The chapter includes comparison between the measurements and the simulation data.

This report ends with conclusions and recommendations for further research within the project. These can be found in chapter 6.

Chapter 2

Linear and planar actuator technology

This chapter provides an overview of existing linear and planar actuators, based on permanent magnets. Although the subject of this thesis is a *linear* actuator, planar actuators are also considered, because this linear actuator is a predesign for a planar one. Therefore, the operating principles of planar actuators are also interesting. The chapter ends with a description of the initial design of the 3-DoF actuator, its operating principles and a model of the design.

2.1 Linear actuators

The term "Linear actuator" covers a diverse area of machine types. A broad classification of these types is shown in figure 2.1. The actuator under design is an example of a motor with progressive motion with a flat geometry. Moreover, it is a permanent magnet synchronous machine. This means that only this group of linear actuators is interesting for the design, because they use a similar operating principle. Therefore, only these PM synchronous actuators are covered in this section. Many of these actuators exist, but only few have integrated propulsion and suspension. The next subsections provide an overview of structures of linear actuators. The actuators are named after the researchers who developed them. The first sections show machines without suspension by means of repulsive levitation, but in section 2.1.4, an actuator with integrated suspension is described.

Magnetic levitation is the process by which an object is suspended above another object, solely supported by magnetic fields. The electromagnetic force is used to counteract the effects of the gravitational force. Earnshaw's theorem is proved by S. Earnshaw in 1842 [2]. In essence, it states that there is no stable and static configuration of levitating permanent magnets. This means that the forces acting on an object in any combination of gravitational, electrostatic, and magnetostatic fields will make the object's position unstable. However, several possibilities exist to make levitation viable, by violating the assumptions of the theorem. One of those, as will be used for the actuator under design, is using feedback control to position the translator.

When the relevant literature is searched for magnetic levitation, most papers handle about magnetically levitated trains (Maglevs). Although these are described as levitated systems, most of them work upside down: The forces are attractive (stator and translator attract each other) instead of repulsive (stator and translator

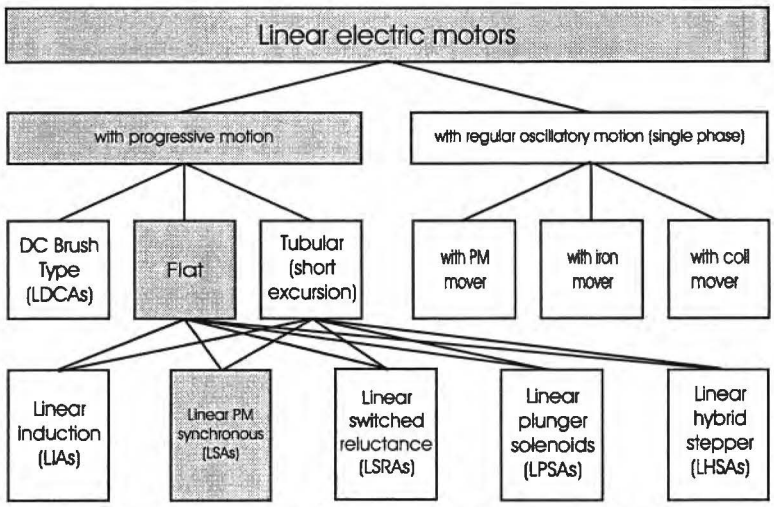

Figure 2.1. *A broad classification of linear machines*

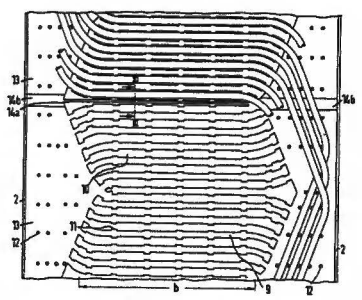

Figure 2.2. *Top view of a stator part (from [3])*

repel each other), making the system not directly comparable to that under design.

2.1.1 Düll (1979)

An early example of a design of an ironless linear motor is a patent by H.J. Düll [3]. It describes a stator for a linear motor, designed to propel rail vehicles. The stator consists of a wave winding placed in a non-magnetic material, as can be seen in figure 2.2. The advantage of a wave winding is that the conductors are close to the air gap and therefore close to the permanent magnets of the vehicle. In this case, the stator is designed to fit in between the existing tracks. Moreover, because of the wave winding, it is possible to install it using prefabricated parts.

This design is a Lorentz actuator: force is created on the current conducting wires because of the magnetic field of the mover. The levitation of the vehicle is not included in the patent, because the design is meant for use with rail vehicles.

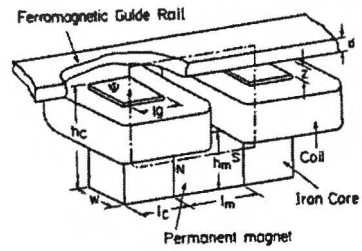

Figure 2.3. *Hybrid magnet perspective view (from [5])*

2.1.2 Morishita (1989)

The article of Morishita et al. [4] describes an electromagnetic suspension system for maglev vehicles. The mover has an iron C-core with a permanent magnet and an electromagnet (see figure 2.3). Due to the permanent magnet, there is always an attractive force between the mover and the ferromagnetic guide rail. The electromagnet is used to increase or decrease this force to control the levitation. A system like this is called a prestressed system.

The system is described as magnetically levitated, although it works upside down, and is therefore based on attractive forces (the stator and mover attract). The force behaves like the force in a normal C- or E-core system, making it inherently unstable. The authors have developed a new control method to minimize power dissipation, the Zero Power Control Method. The gap sensor is a reflecting optical sensor (LED and phototransistor). The power dissipation is about 5 W for levitating 11 kg, most of which is dissipated in the gap sensors.

2.1.3 Wang (1991)

I.Y. Wang et al. developed a magnetic levitation transport path for moving objects in clean environments [5]. The purpose of this design is to prove that levitation with a passive carrier (equipped with permanent magnets) is possible. In their experiment with a mover of only 0.98 cm by 0.98 cm, they did not succeed in achieving complete levitation.

The transport path can be seen in figure 2.4. The mover (carrier) has four permanent magnets. The stator consists of 6 wires which are wound around an aluminium block. Applying current to subsequential wires will result in a propulsion force on the mover.

The advantage of this geometry is that the carriers can move both above and underneath the stator. However, the disadvantage is that half of the winding produces very little force on the carrier. The maximum speed of this magnetic levitation transport path is 0.27 m/s for a carrier mass of 0.176 gram. It would be interesting to see the power that is required for suspension of the carrier, but unfortunately this performance index is not mentioned in the paper.

2.1.4 Yoshida (2002)

One of the more recent designs is presented by K. Yoshida et al.[6]. A pass-through section for the maglev vehicle ME03 was designed that provides both suspension

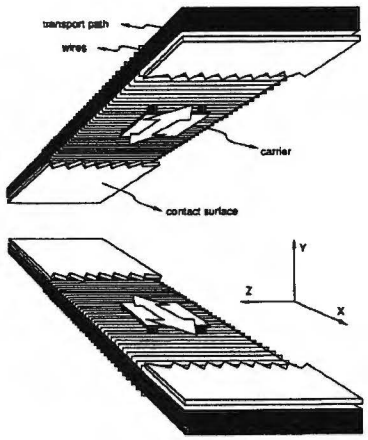

Figure 2.4. *Hybrid magnet perspective view (from [4])*

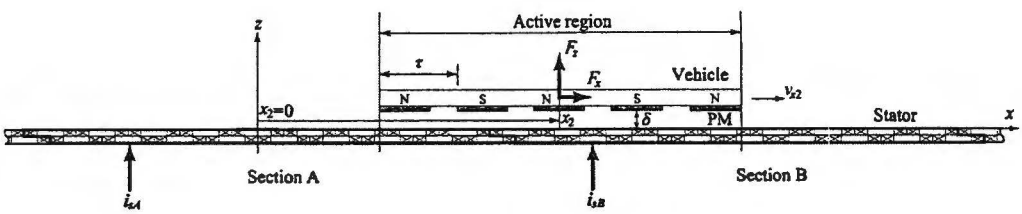

Figure 2.5. *Combined propulsion and levitation PM LSM system (from [6])*

and propulsion. The goal of the research was to achieve smooth movement between two identical sections (A and B), as can be seen in figure 2.5

The permanent magnet linear synchronous motor has "air-cored" windings in the stator and permanent magnets mounted on the vehicle in a simple north-south configuration (see figure 2.5). This configuration can produce force in both x- (propulsion) and z- (suspension) directions. Although most maglev systems are based on attractive levitation, this is based on repulsive levitation, and is therefore interesting for this thesis.

It would be interesting to know the specifications of this actuator. Unfortunately, few details are mentioned in the paper: the maximum speed is 0.5 m/s with a vehicle of 47 kg. The levitation system was capable of reducing the mass by 25 kg, using a current of 4.3 A.

The authors propose a new direct-torque-control (DTC) system in mass-reduced-mode to achieve smooth movement of the vehicle. Experiments have confirmed that this DTC system is indeed capable of creating smooth movement.

2.2 Planar actuators

An overview of planar actuator technology is presented by J.W. Jansen in [7]. Additionally, it is wise to review new designs, as well as some extra types of planar

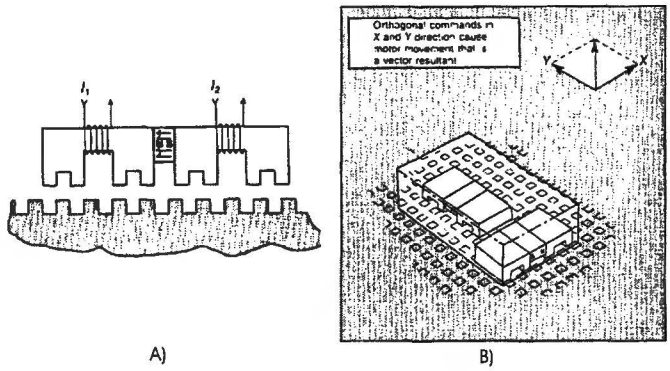

Figure 2.6. *Structure of surface actuator: A) Forcer B) Overview (from [9])*

actuators that are not described in that publication. As with the linear actuator, designs using techniques not based on permanent magnets are also not reviewed, because they are beyond the scope of this thesis.

2.2.1 Pelta (1987)

One of the oldest planar motors was invented by B.A. Sawyer in 1968 [8]. In 1987, E.R. Pelta described a two-axis Sawyer motor for motion systems [9].

The platform has two forcers (components that create force in a certain direction) to be able to move in both the x- and y-directions. The stationary part is made of magnetic material and has a "waffle" structure (see figure 2.6). A mover consists of a number of poles that are energized successively to create movement. It also contains a permanent magnet to force the mover into a certain position. As can be seen from figure 2.6, successively energizing I_1 and I_2 will create movement (away from the stable position), therefore forming a reluctance actuator. By means of two (or four) forcers on the moving platform, this machine can have three DoF: movement in x- and y- directions and rotation around z-axis.

Sawyer motors have a good open-loop positioning capability and high speed. However, repulsive levitation and more than three DoF within one actuator is impossible.

2.2.2 Flores Filho (1999)

The planar motor designed by A.F. Flores Filho et al. [10], which can be seen in figure 2.7, has a topology that is fairly different from the Sawyer motors. It has a slotless stationary part with coils wound around it in x- and y- directions. The mover consists of two NdFeB permanent magnets connected via a back iron "bridge". This actuator can move in two DoF and levitation is not included. Therefore, the mover is supported by mechanical bearings (the "trucks" in figure 2.7).

The mover is propelled by energizing successive coils in a certain direction. Unlike other designs, the mover cannot rotate around the z-axis (which is usually the third DoF) because of the coil topology. Also, the authors experienced large end-effects, which influence the performance of the machine.

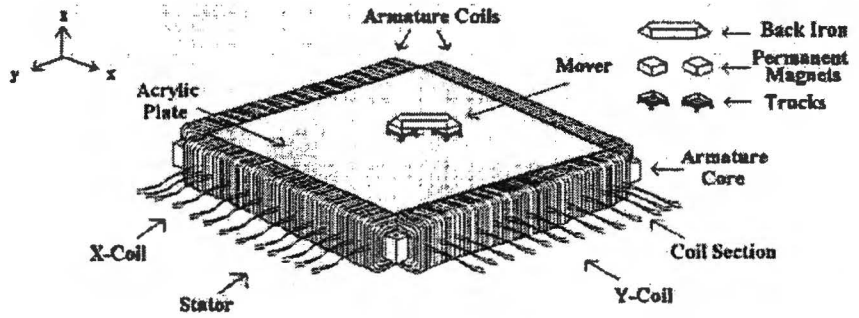

Figure 2.7. *Perspective view of the planar actuator (from [10])*

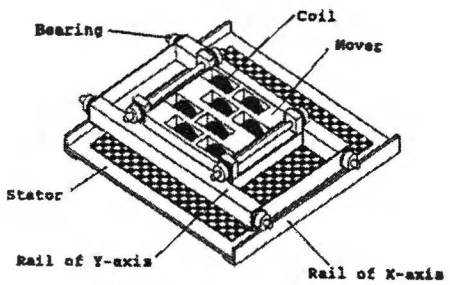

Figure 2.8. *Structure of surface actuator (from [11])*

2.2.3 Ebihara (1992)

D. Ebihara et al. have developed one of the first x-y drives that has only one motor instead of two [11]. Figure 2.8 shows that the mover is equipped with iron C-cores with coils (the electromagnets), and that it is supported by a gantry. The permanent magnets on the stator plane are placed in a simple north-south configuration. Movement occurs when the mover coils are energized successively.

The device is named surface motor instead of planar motor, probably because levitation is not implemented in this design, as can be seen from the presence of iron in both stator and mover. Therefore, the design is not comparable to this of the IOP-EMVT planar motor.

2.2.4 Markle (1999)

D.A. Markle invented a planar motor that provides movement in x- and y- directions as well as suspension in z-direction [12]. It has Halbach magnet arrays on the moving part, while the stationary part has two sets of flat coils, which are offset 45 degrees with respect to the magnet arrays, and 90 degrees to each other (see figure 2.9). These two coil sets can provide force in both x-, y- and z- directions. However, one of the coil sets is inevitably further away from the mover in z-direction, therefore requiring more current density to achieve the same force on the magnets.

As can be seen in figure 2.10, the invention was designed as a wafer support.

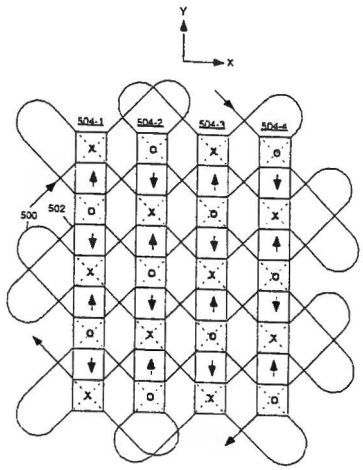

Figure 2.9. *Configuration of magnet arrays and coils (from [12])*

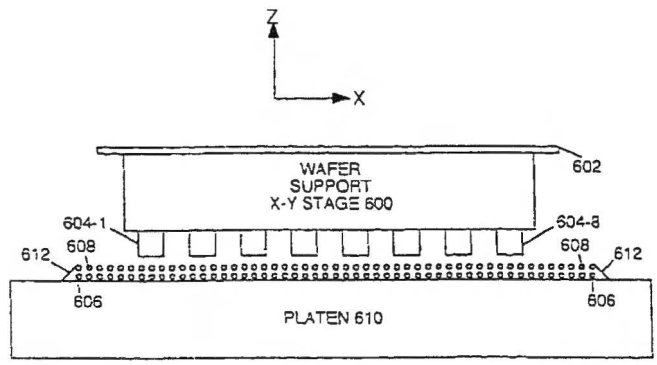

Figure 2.10. *Embodiment of the invention (from [12])*

The patent claims that the invention is much more compact and energy efficient than earlier x-y stages that normally consist of four separate drives. Unfortunately, because just the principle is patented, no performance indexes are mentioned.

2.2.5 Cho (2002)

Cho and Jung have investigated a synchronous permanent magnet planar motor (SPMPM) [13]. The machine has four coil sets, two for moving in x-direction and two for moving in y-direction. (see figure 2.11 B)) This means suspension through electromagnetic levitation is not implemented. The mover consists of coils fitted on an iron yoke, while permanent magnets with back iron form the stator.

The authors claim that the magnet layout (see figure 2.11 A) (d)) is an optimized combination of layouts suggested by others (a, b and c). This new layout should solve disadvantages of the other layouts. However, the design is not yet

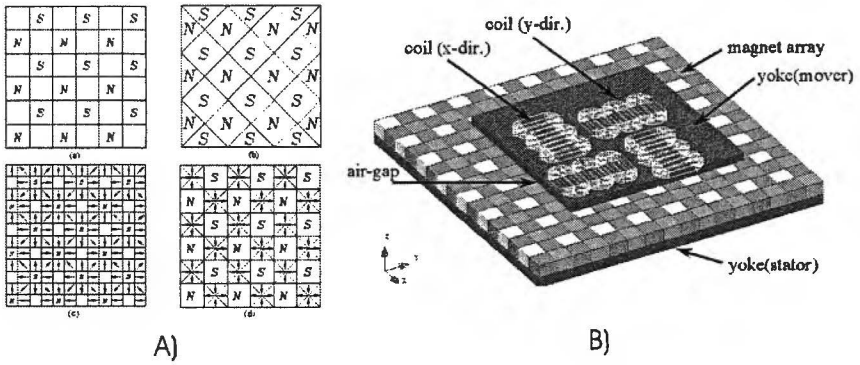

Figure 2.11. *A) Magnet arrays for planar motor (a) Asakawa (b) Chitayat (c) Trumper (d) magnet array proposed by Cho B) Outline drawing of the SPMPM (from [13])*

optimized for parameters such as pole pitch, coil sizes and number of coils, and the cogging force should still be investigated.

2.2.6 Teng (2004)

In 1985, T. Asakawa invented a two-dimensional motor (see figure 2.12) [14]. This machine has a stationary part with an array of coils mounted on back iron and a mover with an array of north-south permanent magnets, also mounted on back iron. As a result, this machine has at most three DoF. The magnetic field of the stator has a sinusoidal shape in both x- and y- directions. The movement is achieved by energizing the three coils as a three-phase system.

In 2004, T. Teng et al. [15] created an actuator based on a similar topology, as can be seen from figure 2.12, and developed a control scheme for this machine. The goal was to decouple the three axes of motion. They succeeded in decoupling linear x- and y- movement, but could not decouple the yaw control yet. This analysis was meant to be an intermediate step in the design of a 6-DoF machine, but because of the back iron in the machine, this can only be made possible by external bearings. (such as air bearings)

2.2.7 Tsuchiya (2004)

J. Tsuchiya and G. Kimura have developed a surface actuator with moving magnets [16]. Therefore, the range of movement is not limited by cables. The structure of the machine can be seen in figure 2.13 A). The mover consists of four permanent magnets, mounted to the corners of an iron plate. The stator is formed by an array of coils on an iron yoke. Movement is possible by energizing the coils adjacent to the current position of the magnets (see figure 2.13 B)).

The back iron on both mover and stator causes attractive force between mover and stator. Therefore, this is a 3-DoF machine (x, y and yaw) and the mover is supported by roller bearings. The authors have measured the torque patterns of the actuator and have obtained the optimum driving pattern for rotational motion (yaw). However, the torque ripple of this machine is quite high, because of the

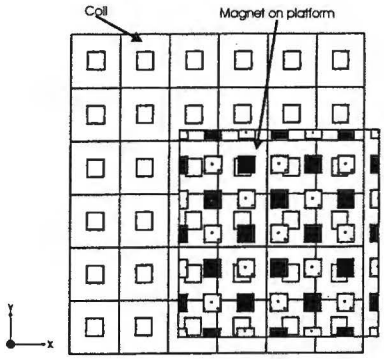

Figure 2.12. *Structure of the Teng-planar motor: magnet plate overlapping the coil plate (from [15])*

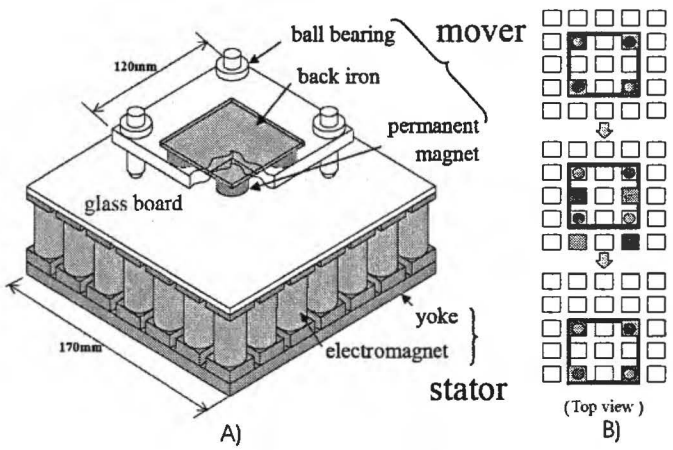

Figure 2.13. *Left: structure of the surface motor Right: linear motion(from [16])*

relatively large poles.

2.3 Evaluation of the overview

Most of the linear actuators mentioned in section 2.1 do not resemble the one required for this project, because they are not coreless, and therefore do not include repulsive levitation. Interesting papers are those by Wang and Yoshida, but both do not state the power dissipated for levitation, which would be an interesting performance index.

The most interesting planar actuator designs are those mentioned by J.W. Jansen in [7]: The moving coil planar motor of Compter and Frissen [17], the moving magnet planar motor of Hazelton et al. [18] and the planar motor of M. Binnard [19].

Most planar motors found in literature (which means those not already discussed in [7]) do not include levitation. Therefore, their concepts are not very

useful for this project and not comparable to the actuator that should be designed here. The design of Markle is interesting, because it does incorporate levitation, in a way that is comparable to the 3-DoF actuator under design. Unfortunately, no performance indexes of the Markle-design are known.

2.4 Starting point for design

2.4.1 Design specifications

As stated in the introduction (chapter 1), the goal of this project is to design an actuator with three DoFs. A number of boundary conditions and limitations are given which the design should meet, as can be seen below. The linear actuator should:

- be useful as a preliminary stage for the design of a 6-DoF planar actuator,
- include magnetic levitation,
- be coreless (ironless),
- be supported by the H-drive available in the lab.

The 6-DoF planar actuator, which is the final goal of the IOP-EMVT project, could be used in lithographic systems for semiconductor production. Therefore, it is desirable to have a Halbach magnet array on the mover, as the presence of magnetic field above the mover is unwanted. A brief explanation of a Halbach array can be found in section 1.3.

2.4.2 Basic geometry

The straightforward way of constructing a magnetically levitated linear actuator with a Halbach magnet array is shown in figure 1.2. It consists of a straight Halbach magnet array and a set of air coils, placed in a straight line. If the distance between the coils matches the translator magnet sizes in the right way (as is explained in section 2.4.4), both levitation and propulsion should be possible with this geometry.

This can be seen by simply applying Lorentz' law to the coil conductors. A coil which is directly below a pole magnet (magnetized in z-direction) will create maximum (positive or negative) suspension force, whereas a coil directly below a longitudinally magnetized magnet (magnetized in x-direction) will produce maximum propulsion force.

The actuator topology mentioned before would meet all specifications, except the one that it should also be useful for estimating the behavior of a planar (6-DoF) actuator version. Therefore, it is interesting to choose a more complicated geometry, where either the coil structure or the magnet array is two-dimensional instead of one-dimensional.

Two different geometries in this category are considered. The first one has a rectangular magnet array with square magnets, but the coils are rotated 45 degrees with respect to the magnets (figure 2.14). Again, the force produced by a coil can be derived by applying Lorentz' law. Applying the same current to both sides of the coil array should result in a stable linear movement. However, it is not very efficient, because y-components of the forces on the two rows of coils are counteractive.

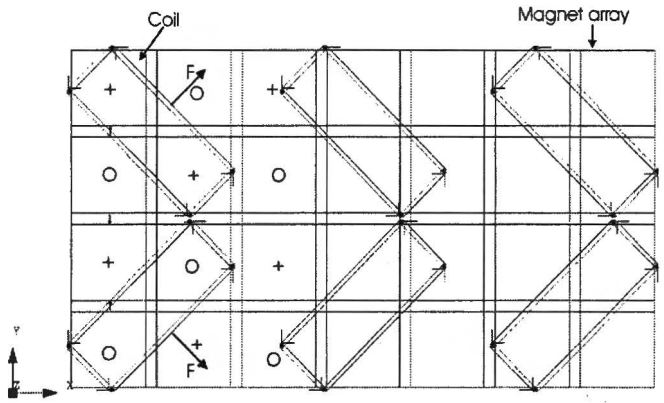

Figure 2.14. *A fish bone structure for a 3-DoF actuator*

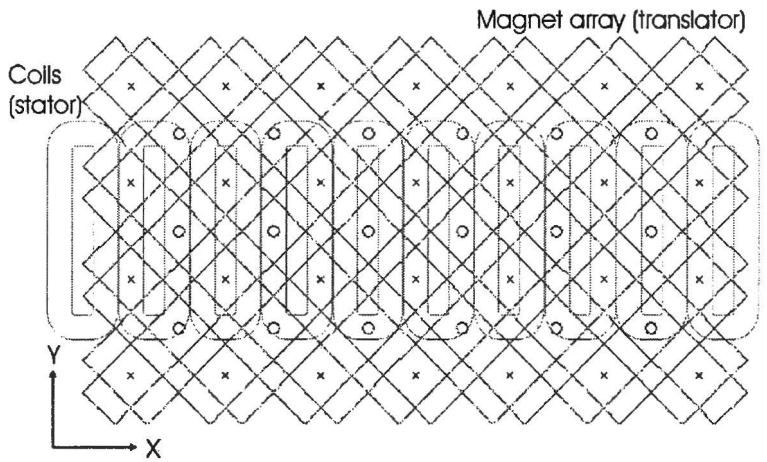

Figure 2.15. *3-DoF actuator with magnets rotated 45 degrees*

The second design has rectangular coils, placed in a straight line. However, now the magnet array is rotated 45 degrees (figure 2.15) with respect to the coils. This geometry is probably harder to model and manufacture, but it is closer to a possible geometry for the planar motor, since it has a two-dimensional magnet structure. Because of this, it is used as the basic geometry to start the optimization from.

2.4.3 Operating principle of the actuator

The magnet array on the translator produces a certain magnetic flux density. This can be split into an x-, y- and z-components (with respect to the magnets). However, as the magnets are rotated 45 degrees with respect to the coils, these components are not perpendicular to the coil conductors. Since only the perpendicular field component is producing force (Lorentz' law, see section 3.3.1), it is more interesting to calculate this.

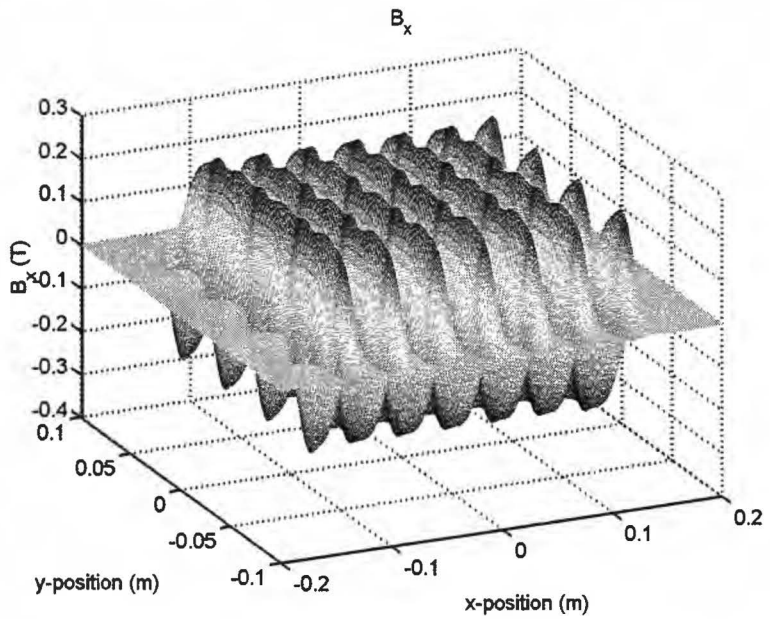

Figure 2.16. *x-component of the flux density*

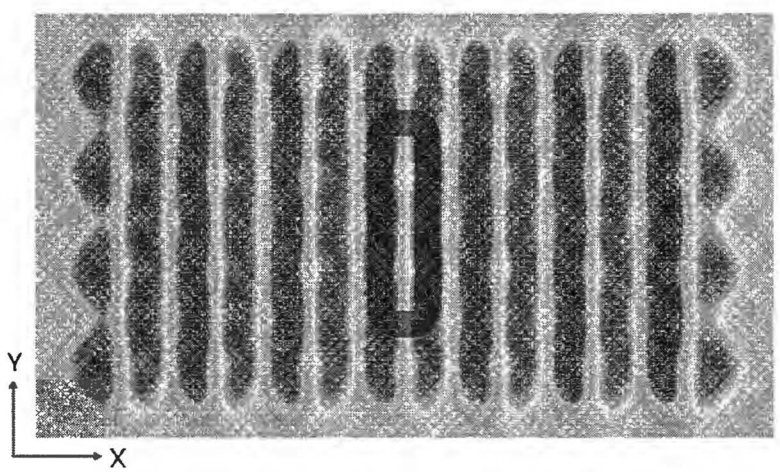

Figure 2.17. *x-component of the flux density, with coil*

The magnet array with the coils in place is shown in figure 2.15. The magnetic flux density component in the x-direction (with respect to the coordinate system shown) is shown in figure 2.16. This component is perpendicular to the long side of the coil. Applying Lorentz' law exhibits that this results in a suspension force in z-direction. Figure 2.17 again indicates the magnetic flux density in the x-direction, but this is a top view, and also illustrates the placement of a coil. Because its conductor bundles are placed symmetrically with respect to the flux density peaks, the force on the left conductor bundle will always be in the same direction as that

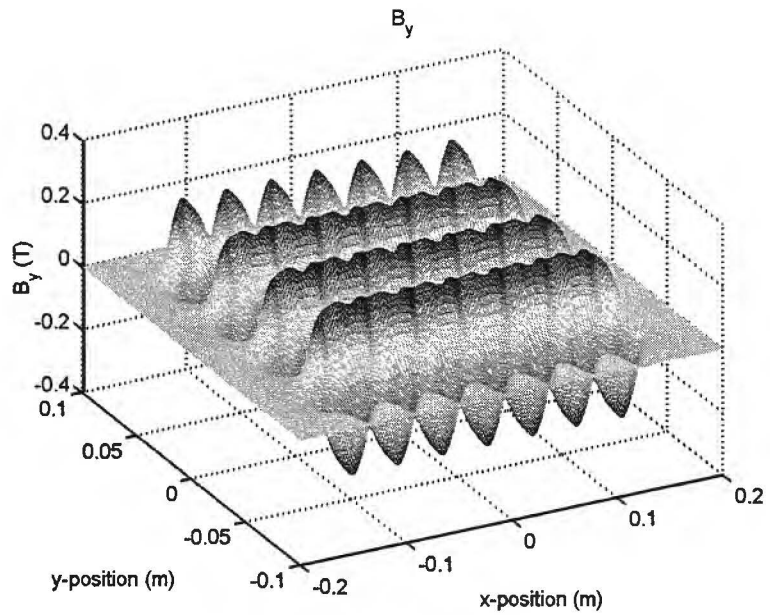

Figure 2.18. *y-component of the flux density*

on the right conductor bundle.

Since the plots are made for an array sized as displayed in figure 2.15, they also display the edge-effects. Along all edges of the array the field components denotes a larger ripple or a line of peaks instead of a more or less flat maximum. The green surface is the area outside the array, where the flux density is of course zero. The width of the array is chosen in such a way that the edge effects along this side are outside the coil array. However, during long stroke motion, the edge effects along the short side pass over coils. This has to be taken into account when the actuator is operated and controlled.

The magnetic flux density component in y-direction (as shown in the figure) can be seen from figure 2.18. Again, applying Lorentz' law explains that this component creates force in z-direction on the short sides of the coil. If these forces were unequal, this would result in a roll (rotation around the x-axis), providing that this DoF is not mechanically locked. This can be avoided by placing both short sides of the coil in a position where the y-component of the field is equal to zero. This coil placement is demonstrated in figure 2.19, also representing a top view of the y-component of the flux density.

The force to propel the actuator (move it in x-direction) has to act on the long sides of the coil. From Lorentz' law, it can be seen that the z-component of the magnetic flux density is responsible for this force. This z-component, shown in figure 2.20, is not as smooth as those in x- and y-directions. However, by placing the coil as is shown in figure 2.21, the force distribution is symmetrical, therefore not introducing a disturbance torque.

The above proves that it is possible to create force in both x- and z-directions with this actuator geometry. The next section describes the placement of the successive coils in x-direction, because this influences the way the actuator can be

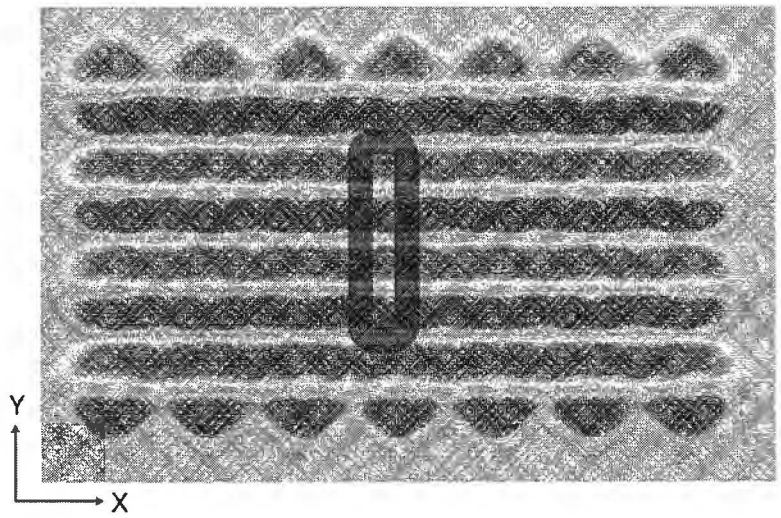

Figure 2.19. *y-component of the flux density, with coil*

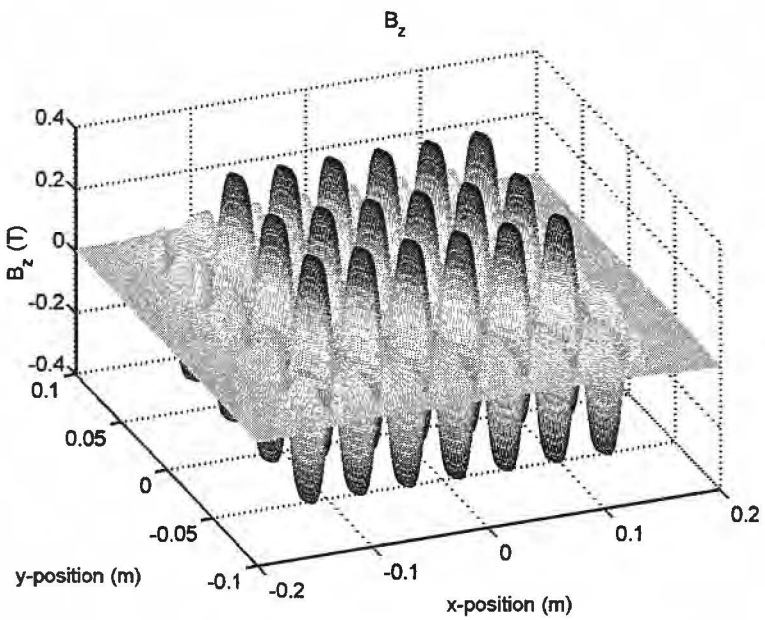

Figure 2.20. *z-component of the flux density*

controlled.

2.4.4 Number of phases

Although the actuator under design can probably not be described as a symmetrical n-phase system (with n an arbitrary integer), the term *number of phases* is used to clarify the operating principle. For instance, if the system were a three-phase one,

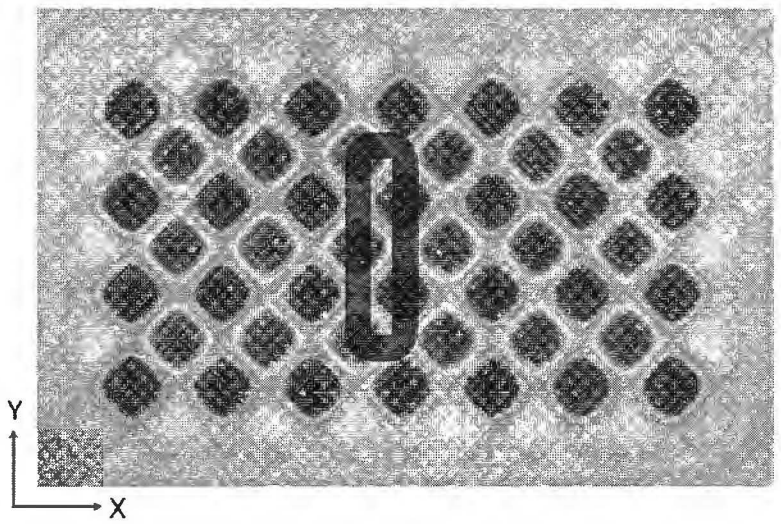

Figure 2.21. *z-component of the flux density, with coil (responsible for F_x)*

three energized coils would be required to provide position independent suspension and propulsion forces. To be able to control the torques on the translator as well, double the number is required, which means this would essentially result in a six-phase system.

Considering the maximum sizes of the machine (further explanation is given in chapter 4), it is wise to choose the minimum number of energized coils that is capable of both moving the translator into every position and controlling the torques. A two-phase system has only two energized coils to support the translator and it is therefore unable to move the translator in every position. Thus, a four-phase system is the smallest number and seems to be the best option. This means that four energized coils are needed to support and control the translator: two coils (out of four) should be in lifting position, and two should be in propulsion position.

The translator pole pitch τ_m is defined as the distance between the center of a north pole magnet to a south pole magnet. However, now that the magnets are rotated 45 degrees with respect to the coils, this definition might not be straightforward to see, as the north- and south poles are not in line with the coils. This is illustrated in figure 2.22.

Therefore, according to the definition, the translator pole pitch equals:

$$\tau_m = \frac{WM + HB}{\sqrt{2}} \tag{2.1}$$

with WM the width of the pole magnets and HB the width of the longitudinally magnetized magnets.

To have two coils out of four in suspension position (and two in propulsion position), and to leave space for the coil conductors as well, the stator pole pitch τ_s is set to 1.5 times the translator pole pitch τ_m. This means a series of four successive coils is able to propel and levitate the translator, and has the ability to control the torques. As a result of this, the minimum size of the translator (not considering magnet edge effects) is set by four times the stator pole pitch and thus equal to 6 $\tau_m = 4\tau_s$. Both τ_m and τ_s are depicted in figure 2.24.

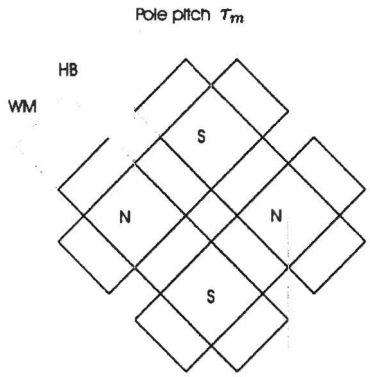

Figure 2.22. *Pole pitch of the magnet array* τ_m

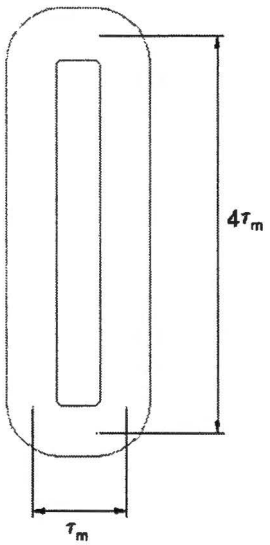

Figure 2.23. *Sizes of the coil in terms of pole pitch* τ_m

Now that the pole pitches are defined, it is possible to define the sizes of the coil in terms of this pole pitch τ_m. In section 2.4.3, it is shown that the long sides of the coil should both be at the maximum value of the flux density component B_x. This means the distance between the conductor bundle centers is equal to τ_m. The short sides of the coil should be in a position where the y-component of the field is zero. The distance between these positions is also τ_m. However, a square coil would not have an equally distributed force in x-direction. Therefore, the space between the short sides of the coil (or the coil length) should be $2n\tau_m$ and is chosen to be $4\tau_m$. This is illustrated in figure 2.23.

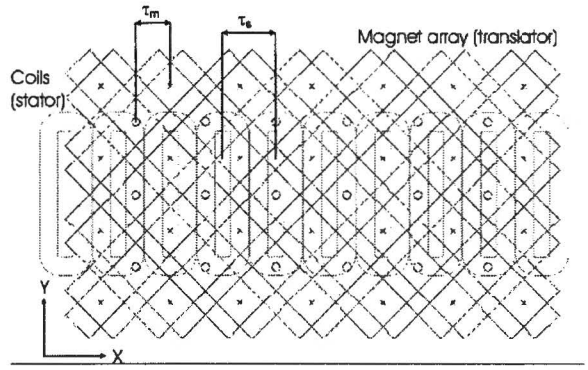

Figure 2.24. *Pole pitches τ_m and τ_s of the actuator*

2.4.5 Force- and current waveforms

The general voltage equation for a coil is:

$$\mathbf{V} = Ri + \frac{d\vec{\psi}}{dt} = Ri + \frac{d\vec{\psi_0}}{dt} + L\frac{di}{dt}, \tag{2.2}$$

with R the resistance of the coil, I the current in the coil and $\vec{\psi}$ the flux. This flux consists of a contribution from the magnets, $\vec{\psi_0}$, and the flux produced by the coil, Li. Assuming movement in only x-direction, the second term can be written as:

$$\frac{d\vec{\psi_0}}{dt} = \frac{\partial\vec{\psi_0}}{\partial x}\frac{dx}{dt}. \tag{2.3}$$

Multiplying this equation by the coil current i gives the total power in the coil:

$$\mathbf{V}i = Ri^2 + \frac{\partial\vec{\psi_0}}{\partial x}\frac{dx}{dt}i + \frac{1}{2}L\frac{di^2}{dt}, \tag{2.4}$$

Then, the first component is the dissipation in the coil, while the third component is the stored magnetic energy. The second term represents the mechanical power. Mechanical power is defined as force times speed, thus:

$$P_{mech} = \mathbf{F}\mathbf{v} = \frac{\partial\vec{\psi_0}}{\partial x}\frac{dx}{dt}i. \tag{2.5}$$

Because the speed is the derivative of the position, $\frac{dx}{dt}$, this means that the force must be equal to:

$$\mathbf{F} = \frac{\partial\vec{\psi_0}}{\partial x}i. \tag{2.6}$$

In the previous section, it is stated that two neighboring coils can suspend and propel the translator. For normal operation, such a pair of coils should be able to produce a constant force in both x- and z-directions. From section 2.4.3, it is clear that the actuator should have a sinusoidal flux distribution. Thus, the flux in x-direction at a certain value of z can be described as:

$$\psi_x = \psi_0 sin\left(\frac{\pi x}{\tau_m}\right), \tag{2.7}$$

then the flux in z-direction can be approximated as:

$$\psi_z = \psi_0 cos\left(\frac{\pi x}{\tau_m}\right), \tag{2.8}$$

where ψ_0 is the amplitude of the flux, x is the position and τ_m is the translator pole pitch. The force component F_x is thus the derivative of equation 2.8, while the force component F_z is the derivative of equation 2.7.

Knowing this, a current waveform that produces a constant force can be derived. Choose the coil current i_1 in coil 1 to be:

$$i_1 = \hat{I}_x sin\left(\frac{\pi x}{\tau_m}\right) + \hat{I}_z cos\left(\frac{\pi x}{\tau_m}\right) \tag{2.9}$$

then for F_x, coil 1 produces:

$$F_{x,1} = -\psi_0 \frac{\pi}{\tau_m} sin\left(\frac{\pi x}{\tau_m}\right)\left(\hat{I}_x sin\left(\frac{\pi x}{\tau_m}\right) + \hat{I}_z cos\left(\frac{\pi x}{\tau_m}\right)\right). \tag{2.10}$$

Coil 2 is placed 1.5 τ_m further in x-direction. Therefore, ψ_z for this coil is a cosine instead of the sine. The current i_2 in coil 2 is chosen to be:

$$i_2 = \hat{I}_x cos\left(\frac{\pi x}{\tau_m}\right) - \hat{I}_z sin\left(\frac{\pi x}{\tau_m}\right). \tag{2.11}$$

The force $F_{x,2}$ that coil 2 produces can then be written as:

$$F_{x,2} = -\psi_0 \frac{\pi}{\tau_m} cos\left(\frac{\pi x}{\tau_m}\right)\left(\hat{I}_x cos\left(\frac{\pi x}{\tau_m}\right) - \hat{I}_z sin\left(\frac{\pi x}{\tau_m}\right)\right). \tag{2.12}$$

The total force in x-direction F_x is the sum of $F_{x,1}$ and $F_{x,2}$. Summing equations 2.10 and 2.12 and rewriting gives:

$$F_x = -\psi_0 \frac{\pi}{\tau_m} I_x \left(sin^2\left(\frac{\pi x}{\tau_m}\right) + cos^2\left(\frac{\pi x}{\tau_m}\right)\right) \tag{2.13}$$

Since

$$sin^2(\alpha) + cos^2(\alpha) = 1 \tag{2.14}$$

per definition, F_x can be written as:

$$F_x = \psi_0 \frac{\pi}{\tau_m} \hat{I}_x = constant. \tag{2.15}$$

The resulting F_z is also constant, which can be derived in a similar way. This proves that it is possible to obtain a constant position independent force with this actuator topology.

2.4.6 Modelling of the design

The final design will have a stator which is longer than the translator (since it is a long stroke actuator), therefore having, for instance, 10 coils. An electromagnetic analysis by finite element modelling of the total actuator structure would result in

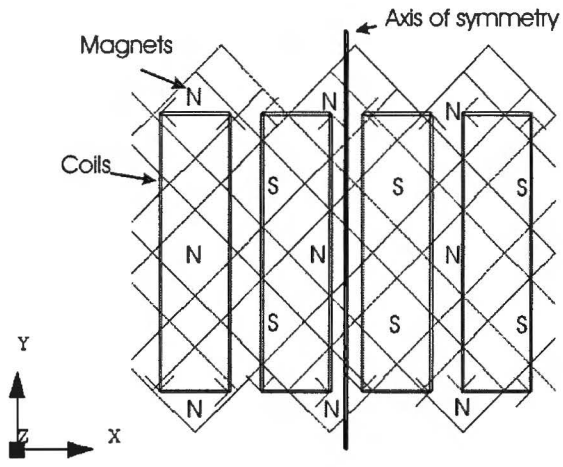

Figure 2.25. *Model reduction due to the symmetry*

a very large model, causing the calculation time to be very long. However, it is not necessary to model the total translator and stator.

As mentioned in the section 2.4.4, the translator is suspended and propelled by four subsequent coils. Because of the placement of the coils, this geometry is symmetrical (see figure 2.25). Therefore, only two coils need to be modelled, the other two are in the same relative position, and thus have the same force per current specification. Moreover, it is also not required to model the total translator. The size of the translator model is chosen in such a way that the two coils experience no edge effects in the position which is chosen for the simulation. In practice, the array will be sized so that energized coils do not experience edge effects.

Therefore, only two coils and a small "piece" of the translator will be considered during simulations. The implementation of the FEM model that is used is described in section 3.6.

2.5 Conclusion

The relevant literature is searched for linear and planar actuators based on the permanent magnet synchronous motor principle. Few actuators provide both suspension and propulsion within one actuator. Only the designs of J.C. Compter et. al., M. Binnard and D.A. Markle show such a configuration. This underlines that this IOP-EMVT project is indeed state-of-the-art research.

Three design options for the 3-DoF actuator are presented. The final design choice will have a stator with coils placed in a straight line. The translator will have an array of magnets, rotated 45 degrees with respect to the coils. This forms a two-dimensional magnet array, which behavior is interesting for the eventual 6-DoF planar motor. Four energized coils will be used to support the translator, but because of symmetry, only two need to be considered in the model.

Chapter 3

Electromagnetic theory of the actuator

The calculation of the magnetic field and related quantities is a difficult process, for instance because of the nonlinear aspects of these calculations when iron is involved or because of the widely spread magnetic field when air coils are used. Therefore, the finite element method (FEM) analysis is an often used method to calculate and predict the electromagnetic behavior of a machine. The general disadvantage of this method is that the calculation time is long. Calculating the behavior by using analytical equations is usually much faster, but can be less accurate.

This chapter describes the main principles of the electromagnetic calculations used in this project, starting from Maxwell's equations. Next, an analytical method to calculate the magnetic field of permanent magnets is treated, followed by a description of the different methods to calculate the magnetic force on a coil conductor. After that, calculation of the inductance of the coils is discussed. The last section concerns the software packages that are used within this project.

3.1 Magnetic field

All macroscopic electromagnetic phenomena are described by Maxwell's equations. In differential form, these are [20]:

Faraday's law:

$$\nabla \times \mathbf{E} = -\frac{\partial \mathbf{B}}{\partial t}, \tag{3.1}$$

Ampère's law:

$$\nabla \times \mathbf{H} = \frac{\partial \mathbf{D}}{\partial t} + \mathbf{J}, \tag{3.2}$$

Gauss's law:

$$\nabla \cdot \mathbf{D} = \rho, \tag{3.3}$$

Gauss's law - magnetic:

$$\nabla \cdot \mathbf{B} = 0, \tag{3.4}$$

Equation of continuity:

$$\nabla \cdot \mathbf{J} = -\frac{\partial \rho}{\partial t}. \tag{3.5}$$

The quantities $\mathbf{D}$ and $\mathbf{E}$, and $\mathbf{B}$ and $\mathbf{H}$ are related by the material properties as follows:

$$\mathbf{D} = \varepsilon_r \varepsilon_0 \mathbf{E}, \tag{3.6}$$

$$\mathbf{B} = \mu_r \mu_0 \mathbf{H}. \tag{3.7}$$

or

$$\mathbf{B} = \mu_0(\mathbf{H} + \mathbf{M}) \tag{3.8}$$

with $\mathbf{M}$ the magnetization.

For static fields (meaning there is no time variation), as are used in magnetostatic Finite Element calculations, these differential equations can be simplified and written as:

$$\nabla \times \mathbf{E} = 0, \tag{3.9}$$

$$\nabla \times \mathbf{H} = \mathbf{J}, \tag{3.10}$$

$$\nabla \cdot \mathbf{J} = 0. \tag{3.11}$$

Equations 3.3 and 3.4 do not change in the static case.

Maxwell's equations can be solved directly for the fields. However, it is often more convenient to obtain the fields using potential functions. This is described in the next section.

3.1.1 Magnetic potentials

To solve the Maxwell's equations, the four coupled first-order differential equations involving two field quantities are converted into a pair of uncoupled second-order differential equations with only one field quantity. For the magnetostatic field, this is achieved by defining the magnetic vector potential $\mathbf{A}$. Equation 3.4 can be satisfied by defining:

$$\mathbf{B} = \nabla \times \mathbf{A}. \tag{3.12}$$

Substituting this equation into the static Ampère law (equation 3.10) results in the following second-order differential equation:

$$\nabla \times \left(\frac{1}{\mu_0 \mu_r} \nabla \times \mathbf{A} \right) = \mathbf{J}. \tag{3.13}$$

This magnetic vector potential has to be calculated to obtain both the inductance of the coils and the force they excite on the magnets (if the Virtual Work or Maxwell Stress method is used). Another potential that is often used by FEM software is the scalar potential, defined as:

$$\mathbf{B} = -\nabla \cdot \phi, \tag{3.14}$$

with ϕ the scalar potential. Because equation 3.4 states that there are no magnetic monopoles, ϕ satisfies Laplace's equation:

$$\nabla^2 \cdot \phi = 0. \tag{3.15}$$

This can be written as a Laplace series to find the solution.

By making this change of variables to either the vector potential $\mathbf{A}$ or the scalar potential ϕ, the uncoupled magnetostatic and electrostatic equations along with their constitutive relations can be solved independently for the magnetic and electric fields [21].

3.1.2 Finite Element Method approach

The Finite Element Method (FEM) is a numerical procedure to find the solution to a boundary value problem [20]. The boundary values for electromagnetic problems can be derived from Maxwell's equations, giving the field continuity equations, such as for an interface between two media 1 and 2:

$$u_n \times (\mathbf{H}_1 - \mathbf{H}_2) = 0 \tag{3.16}$$

and

$$u_n \cdot (\mathbf{B}_1 - \mathbf{B}_2) = 0 \tag{3.17}$$

with u_n the unit normal vector, $\mathbf{H}_1$ and $\mathbf{H}_2$ the magnetic field strength in medium 1 and 2, respectively. Also, $\mathbf{B}_1$ and $\mathbf{B}_2$ are the magnetic flux density in medium 1 and 2, respectively.

Now that the boundary values are known, the finite element analysis can be performed in four steps:

- Discretization (subdivision) of the domain,
- Selection of the interpolation functions,
- Formulation of the system of equations,
- Solution of the system of equations.

Discretization is a critical step in FEM analysis. It involves dividing the domain into smaller domains, usually called *elements*. The total subdivision is called *mesh*. The elements are often triangular in 2D FEM, or tetrahedra or triangular shaped prisms for 3D FEM. The problem is formulated in terms of the unknown function ϕ at nodes (i.e. the corners of a tetrahedron) of the elements. The size of the elements has to be picked very carefully and should depend on the gradient of the field in the region. For instance, an "air gap" region, between coils and permanent magnets, will have a high field gradient and therefore requires a high element density.

Selection of the interpolation functions is the second step of FEM analysis. The unknown solution within an element is approximated by a polynomial of at most the fourth order. Higher order polynomials are more accurate, but result in a more complicated formulation.

Next, the system of equations should be formulated. This can be done by either the Ritz method (variational formulation) or the Galerkin method (weighted residual formulation).

The final step is solving the resulting system of equations. This has one of the following forms: either

$$[K]\phi = \mathbf{b} \tag{3.18}$$

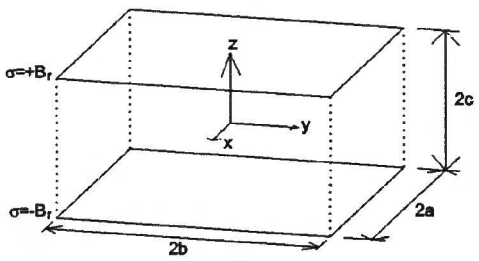

Figure 3.1. *Permanent magnet magnetized in positive z-direction*

or

$$[A]\phi = \lambda[B]\mathbf{b} \tag{3.19}$$

The first equation is of the deterministic type, while the second is of the eigenvalue type. After the system has been solved for ϕ, it is possible to calculate the required results, such as inductance, impedance and force, using the potential functions described in the previous section.

3.1.3 Field of cuboidal magnets

Modelling permanent magnets means substituting the analyzed permanent magnet system with another non-permanent magnetic system so that both systems are magnetically equivalent. Different methods for the analytical analysis of 3-dimensional magnet structures can be found in literature:

- Surface current modelling
- Surface charge modelling

The first method is used in many studies, such as [22] and [13]. With this method, the permanent magnets are modelled by equivalent magnetizing currents. Both the current in the coils and the magnetizing currents are described as Fourier series. The magnetic vector potential is obtained from these currents by solving the Poisson equation.

The advantage of this method is that it can be employed for permanent magnets of arbitrary shapes. The major disadvantage of the method is that both coil and permanent magnet arrays are assumed to be infinitely long. Therefore, the end effects cannot be included. Moreover, every significant change in layout of the system requires the formulation of a new Fourier series.

The second method, surface charge modelling, is presented by G.P. Yonnet et al. [23]. This method is only valid for cuboidal magnets, which is its main disadvantage. It models a permanent magnet by two surface charges with opposite polarity on the sides perpendicular to the magnetization direction. However, the end effects of a magnet array can be included with this method, which is a great advantage over the surface current method. Moreover, describing a magnet array is much more simple with the surface charge method.

Figure 3.1 shows a magnet which is magnetized in positive z-direction [24]. Its sizes are 2a, 2b and 2c in x-, y- and z- directions, respectively. The coordinates

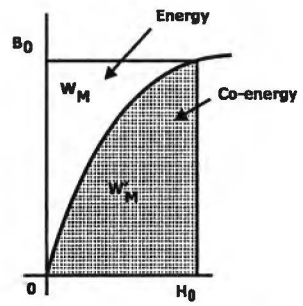

Figure 3.2. *Energy in a magnetic material*

of the center of the magnet are $(u,\ v,\ w)$. The surface charge σ is equal to the remanence of the permanent magnet, B_r.

The flux density in a certain point $(x,\ y,\ z)$ can be calculated by adding the magnetic field contribution of the two opposite surface charges. When a magnet array is considered, the total magnetic flux density can be found by summing the flux density contributions of all individual magnets in the array. The field of one magnet is described by equation 3.20 [24], where the relative permeability μ_r is assumed to be equal to one, both inside and outside the magnet.

$$\begin{aligned} B_x &= \sum_{i=0,1}\sum_{j=0,1}\sum_{k=0,1}(-1)^{i+j+k}\ln(R-T), \\ B_y &= \sum_{i=0,1}\sum_{j=0,1}\sum_{k=0,1}(-1)^{i+j+k}\ln(R-S), \\ B_z &= \sum_{i=0,1}\sum_{j=0,1}\sum_{k=0,1}(-1)^{i+j+k}\mathrm{atan2}\Big(\frac{ST}{RU}\Big). \end{aligned} \tag{3.20}$$

where "atan2" is a four-quadrant arctangent function and:

$$\begin{aligned} R &= \sqrt{S^2+T^2+U^2}, \\ S &= (x-u)-(-1)^i a, \\ T &= (y-v)-(-1)^j b, \\ U &= (z-w)-(-1)^k c. \end{aligned} \tag{3.21}$$

3.2 Magnetic energy

To calculate the magnetic force by using the Virtual Work method (see section 3.3.2), calculation of the magnetic energy is required. The energy in a magnetic material depends on the B-H characteristic of this material. The B-H curve of an arbitrary material is shown in figure 3.2. If this material is operated at values B_0 and H_0 for $\mathbf{B}$ and $\mathbf{H}$, respectively, the magnetic energy density (in J/m^3) is defined as [25]:

$$w_m = \int_0^{B_0} \mathbf{H}\, d\mathbf{B} \tag{3.22}$$

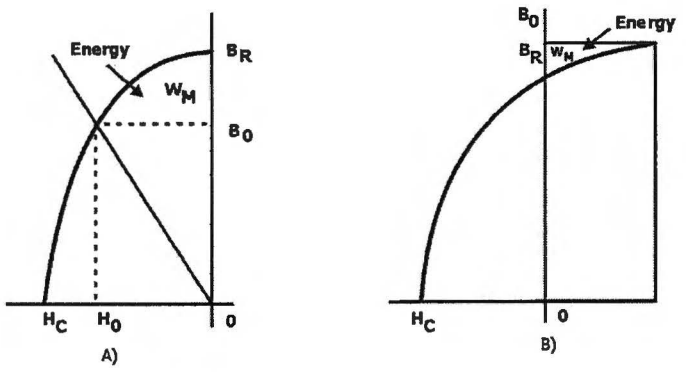

Figure 3.3. *Energy in a magnet: a) stored b) output*

The total magnetic energy in a certain volume, for instance a magnet array, is noted as W_m (in Joule) and is defined as the volume integral of the magnetic energy density ω_m:

$$W_m = \iiint_V \left[\int_0^{B_0} \mathbf{H}\, d\mathbf{B} \right] dV \tag{3.23}$$

This is the area above the B-H curve, marked W_m in the figure. The magnetic co-energy, marked W'_m, is then defined as:

$$w'_m = \int_0^{H_0} \mathbf{B}\, d\mathbf{H} \tag{3.24}$$

The lower boundaries of the integrals in equations 3.23 and 3.24 are the initial conditions of the magnetic field. If for instance iron is considered, these are H=0 and B=0. However, a permanent magnet has an initial state of H=0 and $B = B_r$, with B_r the remanence of the magnet. Equation 3.23 then becomes:

$$w_m = \int_{B_r}^{B_0} \mathbf{H}\, d\mathbf{B} \tag{3.25}$$

If $\mathbf{H}$ is negative, W_m represents output energy. If $\mathbf{H}$ is positive, W_m represents energy stored in the magnet. From the definition of co-energy and the initial conditions then follows:

$$w'_m = \int_0^{H_0} (\mathbf{B} - \mathbf{B}_r)\, d\mathbf{H} \tag{3.26}$$

Figure 3.3 (a) shows the energy a magnet can output (eq. 3.25), while figure 3.3 (b) shows the energy a magnet can store (eq. 3.26), as described by the equations above. These equations can thus be used to calculate the magnetic force.

The only magnetic parts of the coreless actuator under design are the permanent magnets. Therefore, the B-H relation can be assumed linear, making the energy calculation easier.

3.3 Force calculations

In the actuator under design, force is produced when a current is applied to a coil close to the magnet array. There are a number of methods to calculate this electromagnetic force [26]:

- Lorentz force method
- Virtual Work method
- Maxwell Stress method

3.3.1 Lorentz force method

The Lorentz force calculation, based on Lorentz' law, is the most simple method. The force **F** on a indefinitely thin current carrying conductor can be calculated by equation 3.27:

$$\mathbf{F} = (\mathbf{B} \times \mathbf{i})l \tag{3.27}$$

with **B** the magnetic flux density, l the length of the conductor and **i** the current. This can be extended to the "volume force density method", for calculating the force vector on a "thick" conductor or a coil (equation 3.28):

$$\mathbf{F} = \iiint_{V_{coil}} \mathbf{J} \times \mathbf{B}\, dV. \tag{3.28}$$

where **J** is the current density, **B** is the magnetic flux density vector and V_{coils} is the volume.

As this method only requires calculation of the magnetic flux density within the coil volume, this is the fastest method; the calculation time is related to the number of coils and the coil volume. The general disadvantage of this method is that reluctance forces are neglected, but these are not present in the coreless actuator.

3.3.2 Virtual Work method

The concept of Virtual Work may be used to obtain the electromagnetic force acting on a conductor. If a conductor is moved by an infinitesimal distance δx, the work associated is a component of the electromagnetic force F_x in that direction times the distance δx. This work must come from the stored energy of the system W, therefore:

$$F_x = -\frac{\delta W}{\delta x}. \tag{3.29}$$

This means that the total force between elements in a magnetic system can be calculated from the rate of change in total magnetic (co)energy. This is described in section 3.2. The three-dimensional force on the magnet array can thus be obtained by:

$$\mathbf{F} = -\begin{bmatrix} \frac{\partial W_m}{\partial x} \\ \frac{\partial W_m}{\partial y} \\ \frac{\partial W_m}{\partial z} \end{bmatrix}_{\psi=const.} \tag{3.30}$$

or

$$\mathbf{F} = \left[\begin{array}{c} \frac{\partial W'_m}{\partial x} \\ \frac{\partial W'_m}{\partial y} \\ \frac{\partial W'_m}{\partial z} \end{array} \right]_{i=const.} \tag{3.31}$$

In finite element calculations, the derivative can be obtained by calculating the co-energy for the original position and for a small displacement in the direction that is required, while keeping the current in the conductors constant (eq. 3.31). Because the difference between the two obtained values can be very small, this method has to be used with care.

3.3.3 Maxwell Stress method

The Maxwell Stress method is also called the surface integral method, because it obtains the total force by integrating the force density over a closed surface surrounding the magnet array. It considers the value of **H** (the magnetic field strength) on the closed surface to calculate the normal (f_n) and tangential (f_t) components of the force. The general equations for the force per square meter (or force density) are:

$$f_n = \frac{1}{2}\mu_0(H_n^2 - H_t^2) \tag{3.32}$$

$$f_t = \mu_0 H_n H_t \tag{3.33}$$

The total force can then be written as:

$$\mathbf{F} = \iint_S \frac{1}{2}\mu_0(H_n^2 - H_t^2)\mathbf{u}_n \, dS + \iint_S \mu_0 H_n H_t \mathbf{u}_t \, dS \tag{3.34}$$

where u_n and u_t denote the unit vectors in the normal and tangential directions, respectively, to the elemental surface, dS. H_n and H_t are the components of the magnetic field strength vector **H** along those directions.

The danger of this method in finite element calculations is that it can be path-dependent. Choosing a path through the center of gravity (or mid sides) of the elements usually gives good results. Moreover, problems can occur when saturated iron is present, but this will not be a problem as the actuator under design is coreless.

3.4 Inductance

In FEM analysis, the self- and mutual inductance of a coil can be calculated using the magnetic vector potential. The standard equation for the static self inductance is [26]:

$$L = \frac{N}{I}(\mathbf{A}_{a\ mean} - \mathbf{A}_{b\ mean}). \tag{3.35}$$

For the mutual inductance, this is changed to:

$$M = \frac{N_2}{I_1}(\mathbf{A}_{2a\ mean} - \mathbf{A}_{2b\ mean}), \tag{3.36}$$

with $\mathbf{A}_{amean}$ the average magnetic vector potential on leg a, $\mathbf{A}_{bmean}$ the average magnetic vector potential on leg b, N the number of turns of the coil

and I the current in the coil conductors. Index 1 refers to the excited coil, while index 2 refers to the linked coil.

A more accurate way is to integrate the magnetic vector potential along the outside of the coil. The self-inductance is then calculated by:

$$L = \iiint_{coil} \frac{\mathbf{A} \cdot \mathbf{J}}{I^2} dV. \tag{3.37}$$

The mutual inductance can then be defined as:

$$M = N_2 \iiint_{coil2} \frac{\mathbf{A_1} \cdot \mathbf{J_2}}{|I_1||I_2|} dV. \tag{3.38}$$

These formulations can be used to calculate the self-inductance of the actuator coils, because this number has to be known to calculate the voltage over the coils (explained in section 4.2).

It is also possible to determine the "dynamic" self inductance. This is based on the voltage equation for a coil (eq. 2.2). By using this equation, it is possible to include "parasitic" flux contributions from all nearby sources, for instance eddy currents in a conducting plate. This method can be used in simulations and calculations, but also in measurements. In that case, the voltage over the coil can be measured while a sinusoidal current is applied over a certain frequency range.

The "dynamic" mutual inductance can be determined in a similar way. This is done (in practice or in simulations) by energizing one of the coils and recording the induced voltage in the other coil(s). In the geometry of the 3-DoF actuator, the mutual inductance will always lower the total inductance of a coil, because the directions of the coil fluxes are opposite. This means that the inductance calculated using equation 3.37 is the worst-case value.

3.5 Software

A number of software packages are used within this project. This section describes the FEM package and C++ and Matlab codes that are used and what they are employed for.

3.5.1 Finite Element Method software

The finite element software package that is used within the IOP-EMVT project is Flux 2D-3D, version 8.10. This package is manufactured by Cedrat from Grenoble, France.

In this project, the magnetostatic module of Flux 3D is used to check the design and calculate the forces in the final design. The transient magnetic module of Flux 2D is used to calculate eddy currents in the stator. Furthermore, the transient thermal module of Flux 2D is used for a thermal analysis of the designed pre-prototype.

3.5.2 Analytical and numerical software

As mentioned before, finite element software is capable of generating accurate results, but the calculation time is generally very long. Therefore, it can be advantageous to move to simplified analytical methods when a lot of computation steps are necessary.

For this purpose, a software tool in C++ is used, written by J.W. Jansen of the EPE group, that calculates the force on a magnet array. It calculates the electromagnetic field using analytical equations based on the surface charge method (see section 3.1.3) and estimates the force based on Lorentz force calculations. It was published that the results of this program are in good agreement with FEM results [24]. An optimization-program (see appendix A) is written to perform a parametric search that makes use of the force calculation program.

A number of scripts are created in Matlab for visualizing the results of parametric searches and calculating rms values and percentages. These programs can be found in appendix B.

3.6 Model implementation in FEM

The electromagnetic behavior of the final design is verified by Finite Element Method calculations in Flux 3D. Another option to predict the behavior of electrical machines is to use the Magnetic Equivalent Circuit (MEC).

As opposed to the complexity and numerical nature of finite element analysis, the simplicity and analytic properties of magnetic circuit analysis make it the most commonly used magnetic field approximation method for a lot of design work. Two fundamental equations lead to magnetic circuit analysis:

$$\vec{\phi} = \mathbf{B}\, A \tag{3.39}$$

and

$$\mathbf{F} = \int \mathbf{H} dz = \mathbf{H} l \tag{3.40}$$

One of these relates flux density to flux, and the other relates field intensity to magnetomotive force. These equations are connected through the material characteristics. The magnetic circuits can then be described using an analogon to Ohm's law:

$$\mathbf{F} = \vec{\phi} R, \tag{3.41}$$

with R the reluctance of the material, defined as:

$$R = \frac{l}{\mu A} \tag{3.42}$$

with l the length of the path and A the area of the path.

MEC can be a relatively fast way to check the behavior of a machine, but it requires that all magnetic paths are known. If a machine with iron cores is considered, the paths are rather straightforward. However, in an air-cored actuator, as the one under design, all magnetic paths are through air and therefore much more difficult to define. Therefore, using the MEC was not considered as an option for this project.

As with the MEC method, FEM analysis is often used for cored actuators. This means that in most cases, the surrounding air can be neglected, because the permeability of air is much lower than that of iron, resulting in a much higher magnetic resistance. Therefore, the magnetic field will be concentrated in the iron parts. As a result of this, the magnetic paths are well-known, which means it is clear where the densest mesh should be employed.

In Flux 3D, the model has to be surrounded by a rectangular "infinite box". This box is used by the software to set the domain boundaries. Orienting the

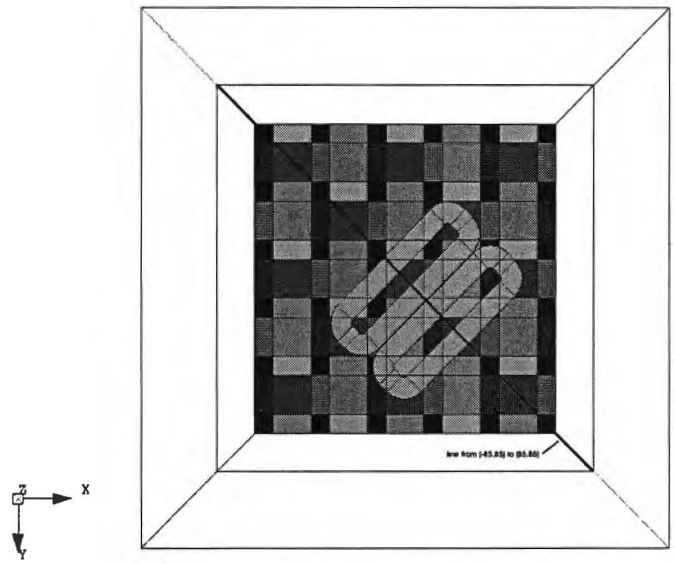

Figure 3.4. *The FEM model (bottom view)*

magnet array as it is in reality would result in a lot of "air" along the sides of the magnets, which has to be meshed and requires calculation time. Therefore, it is more efficient to place the magnet array along x- and y-axes and rotate the coils [7]. The implementation of this is shown in figure 3.4. The drawback is that the force calculation results have to be transformed to another coordinate system to be able to compare them to the analytical results (although this can be done automatically). The model has five pole magnets in both x- and y-directions to eliminate the influence of end-effects on the coils. Only two coils are modelled to decrease calculation time, as is stated in section 2.4.6.

In the 3-DoF actuator, since there is no iron present, the whole region close to the bottom of the magnets, including the coils, should have a dense mesh, because the magnetic field is present everywhere in this region and should be estimated accurately around the coils. Figure 3.5 shows the mesh of the model. The element size on the bottom surface of the magnets is equal to 2 mm, while the coils have elements of 1 mm. This means the "working air gap" (the space in between the magnets and the top of the coils), which is equal to 1 mm, consists of one element layer in z-direction. The top surface of the magnets has an element size of 2.5 mm, because the field gradient is smaller here. A box is placed underneath the array, surrounding the coils. This is used to control the mesh, because otherwise the elements that are relatively far from the coil will become too large. The elements in this box have sides of 3 mm.

These element sizes result in a mesh with approximately 500000 second order elements. Adding more elements makes the model impossible to be solved with the available hardware / software combination. The elements are of the second order, because this is required for the formulation MS3CRTOW, which is used for the air and the coils. This is a formulation in reduced potential with respect to the electric vector potential (referred to as T_o in [27]). The magnet area uses the MS3SCA formulation. This is a scalar potential formulation. Details about these

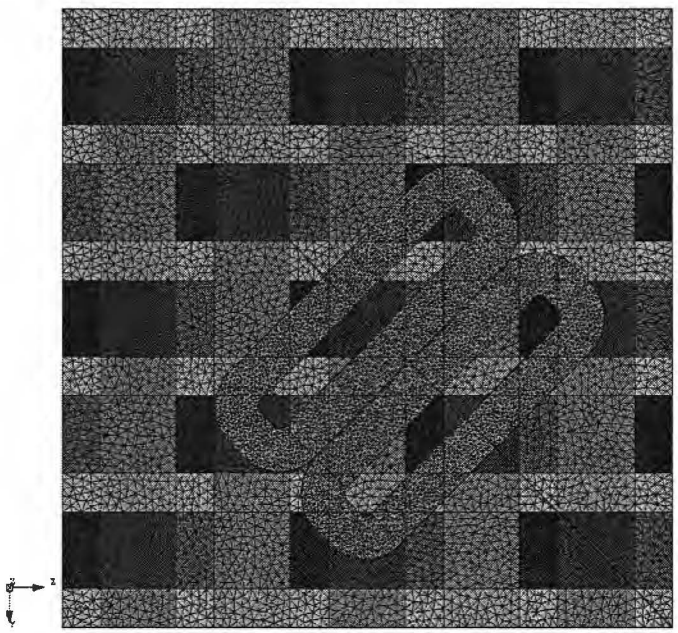

Figure 3.5. *Mesh of the FEM model (two coils and the magnet array)*

formulations can be found in [27].

The model was used to calculate the electromagnetic force by both the Lorentz force and the Virtual Work methods. In most cases it shows good agreement (within 2 percent) with the results obtained from the analytical calculations, but for F_y, which should be equal to zero, the Virtual Work results are alternating around zero. This can be seen in section 4.1.5.

An often used performance index in rotating machines is the *air gap flux density*. Since this 3-DoF actuator contains no iron, there is no real air gap present. However, it is possible to calculate the flux density in the area underneath the magnets, to make a comparison to rotating machines. Figure 3.6 shows the magnetic flux density for the line from (-85,-85) to (85,85) at z=-1 mm (model coordinate system). This means a line parallel to the coil array, passing underneath the centers of pole magnets, 1 mm below the magnets. The peaks in figure 3.6 should all have the same amplitude, because they are directly caused by the permanent magnets. The difference of amplitude values is caused by the discretization of the domain. The airgap flux density waveform in figure 3.6 is totally non-sinusoidal and also not smooth. This is caused by the high field concentration due to the Halbach array structure. Such a flux density will probably introduce force ripples. However, the flux density somewhat further from the magnet array looks a lot more sinusoidal. This is displayed in figure 3.7, which shows the flux density at z= -9 mm. (9 mm below the magnet array). It can be concluded that smooth operation should be possible and force ripples will be limited.

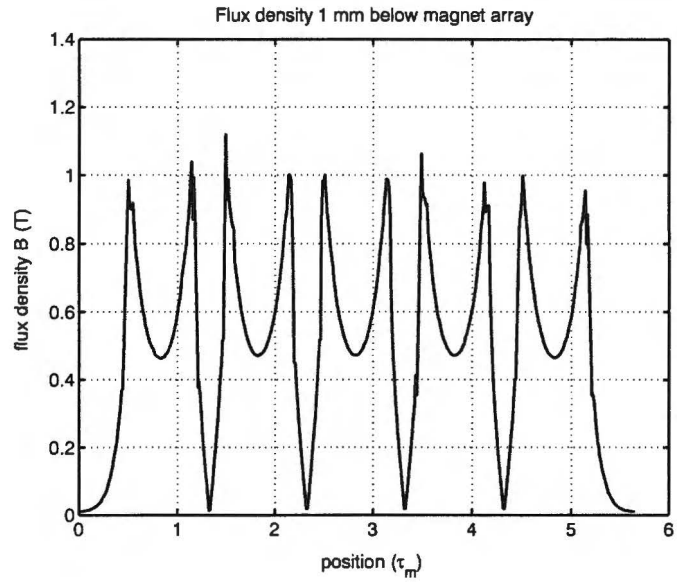

Figure 3.6. *Airgap flux density at 1 mm from the magnets*

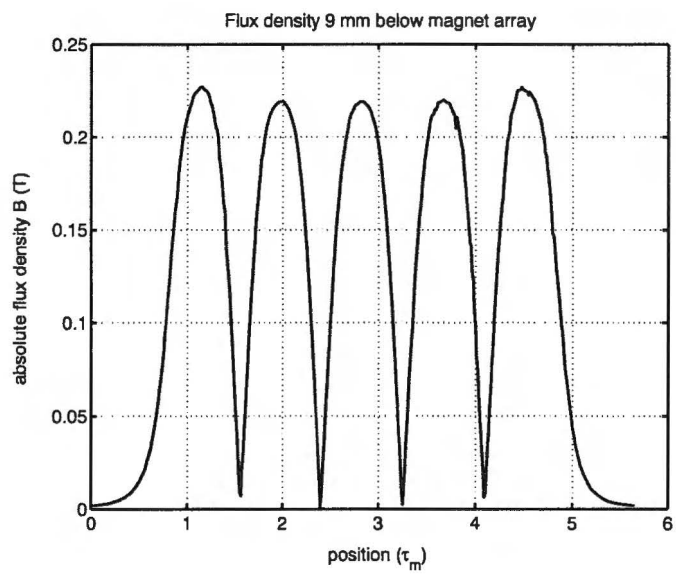

Figure 3.7. *Airgap flux density at 9 mm from the magnets*

Chapter 4
Design flow

Once the global geometry of the design is known (a side view can be seen in figure 4.1), an optimization is employed to find the design which is best to meet all specifications. This chapter describes the steps that are needed to derive this optimal design. The first section describes the optimization process and its results. Next, the calculation of the number of turns per coil is mentioned. The last sections of the chapter describes the disturbances and thermal analysis. The chapter ends with a conclusion, handling about the final design.

4.1 Optimization

4.1.1 Objective

The basic geometry mentioned in section 2.4.2 is not optimal. First, the most important objective for optimization should be specified. In this case, the main objective is to achieve maximum acceleration efficiency in propulsion direction. In other words, the acceleration in x-direction of the actuator for a certain current should be maximized. This means calculation should not only consider the force on the platform, but also its mass. The choice to optimize the acceleration is based on the demands for the planar motor from the semiconductor industry: fast positioning is required.

Furthermore, the force ripple should be minimized to achieve smooth movement, better controllability and lower losses. In essence, this means the flux linkage ψ of the coils should have a waveform that approximates a sinusoidal waveform. Knowing these goals, the following cost functions can be defined:

$$a_x(\mathbf{X}) = max \tag{4.1}$$

$$a_{x,ripple}(\mathbf{X}) = min \tag{4.2}$$

with a the acceleration and $\mathbf{X}$ a vector which contains the geometry variables.

Moreover, the acceleration in z-direction and the ripple on this acceleration should also be sufficient, because the actuator should suspend (levitate) the translator properly and should be able to form a stiff bearing. This introduces two extra cost functions:

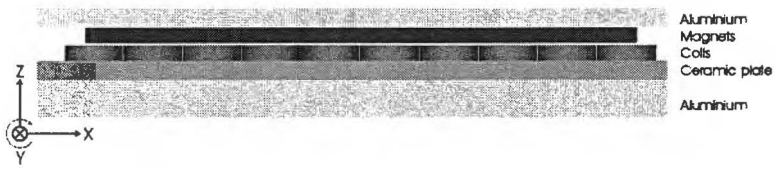

Figure 4.1. *Side view of the actuator*

$$a_z(\mathbf{X}) = max \tag{4.3}$$
$$a_{z,ripple}(\mathbf{X}) = min \tag{4.4}$$

4.1.2 Constraints

As mentioned in section 2.4.2, the design has to meet some practical constraints. For instance, it has to fit in between the legs of the H-drive, meaning the total length must be less than 980 mm. Furthermore, at most 10 amplifiers will be available, limiting the number of coils to 10. This results in the following constraints:

$$L \leq 980\ mm \tag{4.5}$$
$$NA \leq 10 \tag{4.6}$$

where L is the total machine length and NA is the number of power amplifiers. As stated in section 2.4.4, the number of phases that is chosen introduces a constraint for the stator pole pitch τ_s:

$$\tau_s = 1.5\tau_m, \tag{4.7}$$

This sets a limit to the width of the conductor bundle, TH, because this can only be half the maximum size of the coil, which is τ_s, minus 0.5 mm spacing for mechanical tolerances:

$$TH \leq \frac{\tau_s}{2} - 0.5. \tag{4.8}$$

Extra constraints are set by the choice of magnets. The size of the pole magnets determines all other sizes, but it has no effect on the operating principles of the actuator. The height of the magnets mainly influences the strength of the magnetic field. A standard magnet size that the magnet supplier (Bakker Magnetics) had in stock is 20 mm by 20 mm by 8 mm. Because choosing this magnet would result in a machine that can fit in between the H-drive, this size was used to start with, therefore introducing extra constraints:

$$WM = 20mm \tag{4.9}$$
$$HM = 8mm \tag{4.10}$$

with WM the width of the pole magnets and HM the height of the pole magnets. The sizes of the magnets influence the magnetic field. Therefore, the following

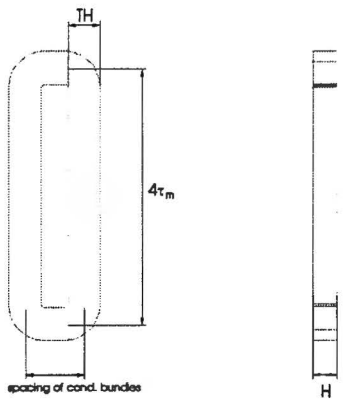

Figure 4.2. *Sizes of the coil*

constraints are also be defined, based on experience:

$$0 \leq HB \leq 20mm \tag{4.11}$$

$$0 \leq H \leq 20mm \tag{4.12}$$

with HB the width of the longitudinally magnetized magnets and H the height of the coils.

4.1.3 Strategy

Having set the pole magnet size and stator pole pitch, a number of variables remains that can be varied, in order to find the optimal design. These are mentioned below. The initial values, based on educated guesses, are printed between brackets. The parameters involving the coils are visualized in figure 4.2

- width of the longitudinally magnetized magnets HB (5 mm),
- width of the coil conductor bundle TH (4 mm),
- height of the coils H (5 mm),
- spacing of the conductor bundle centers ($1x\tau_m$),
- number of turns per coil N (200).

The first four variables influence the force value directly. The number of turns per coil is not influencing the force (assuming constant current density in the conductor bundle area, and thus a constant filling factor), but this number should be adapted to fit the specifications of the power amplifiers. This is described in section 4.2.

Initially, the first four parameters will be used in a parametric search. This means that the resulting designs for different combinations of these parameters will

be checked for their performance on both acceleration and acceleration ripple in x- and z-directions. After that, the number of turns will be adapted to the specifications of the power amplifiers. The order is as follows: first, both HB and TH are varied, because it turned out that they have the largest influence on the acceleration and acceleration ripple. Next, H is varied for the optimal design resulting from the first iteration. Then, the spacing of the conductor bundles is varied.

4.1.4 Tools

To start the optimization, a model of the actuator is needed. The quantities that have to be calculated to derive the acceleration are the forces F_x, F_y and F_z and the mass of the translator m_t. The force calculation was done by a C++ program, written by J.W. Jansen (see [7]). This program takes a few seconds to calculate the forces in one position of the translator, which is why it is much more useful than the finite element software in this case. The mass calculation assumes an aluminium back plate with a thickness of 10 mm.

To calculate acceleration, code was added to include the mass of the translator m_t. (see appendix A) As already mentioned in section 2.4.6, optimization was done for only 2 active coils instead of 10, because of the coil placement.

In general, up to a certain limit, increasing the size of the longitudinally magnetized magnets increases the magnetic field and therefore the force. However, it also leads to the rise of the mass of the translator. This means an optimal value for the size of the longitudinally magnetized magnets can be found.

To be able to find the lowest acceleration ripple, the current waveform should be shaped in such a way that a sinusoidal flux linkage waveform would result in a constant force. This can be achieved by implementing the following equation:

$$i = \hat{I}_x sin\left(\frac{\pi x}{\tau_m}\right) + \hat{I}_z cos\left(\frac{\pi x}{\tau_m}\right) \tag{4.13}$$

The derivation of this equation is explained in section 2.4.5. This equation makes use of the placement of the coils as described in section 2.4.3. When a coil is producing maximum suspension force, it is producing minimum propulsion force, and vice versa. Therefore, the forces F_x and F_z can be decoupled using equation 4.13, where the amplitude $\hat{I}_x$ influences the force F_x and the amplitude $\hat{I}_z$ influences the force F_z

The height of the coils also influences the electromagnetic force. If a constant total current is assumed, an indefinitely thin coil would produce the most force, because in that case the current is closest to the magnets. It is, of course, impossible to have such a coil. Moreover, it is difficult to compare results, because varying the coil height also influences current density in the coils and therefore coil losses.

The same is valid for the width of the coil conductor bundle. Furthermore, another problem occurs: the width of the conductor bundle is limited by the spacing of the coils. This also had to be implemented in the software.

To make a better comparison, the *coil copper losses* are kept constant when the coil height H or coil conductor bundle width TH is varied. Copper losses can be described as:

$$P = I^2 R \tag{4.14}$$

with P the losses, I the conductor current and R the resistance of the coil. Fur-

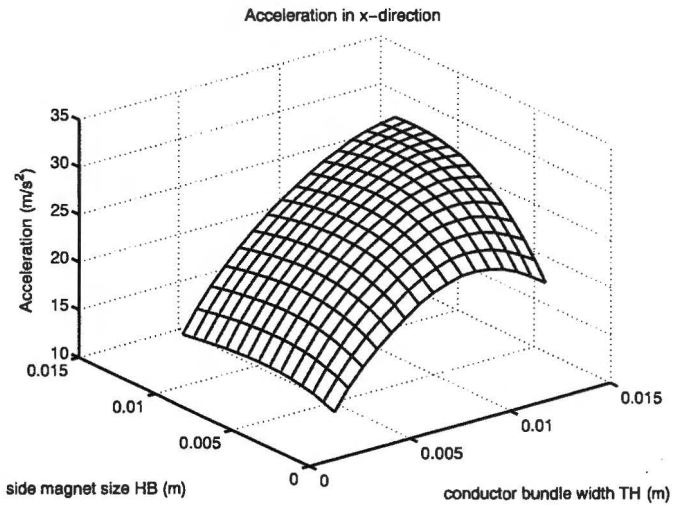

Figure 4.3. *Acceleration in x-direction of the 3-DoF actuator as function of longitudinally magnetized magnet size and conductor bundle width*

thermore, the resistance of a conductor (bundle) is defined as:

$$R = \frac{\rho l}{A} \tag{4.15}$$

with ρ the resistivity of the conductor material, l the length of the conductor and A the area of the cross-section of the conductor (bundle). With parameters TH en H, it is clear that $A = TH \cdot H$. The losses can thus be kept constant by implementing the next equation:

$$P_{rel} = \frac{I^2}{H \cdot TH} \tag{4.16}$$

and therefore

$$I = \sqrt{\frac{P_{rel}}{H \cdot TH}} \tag{4.17}$$

P_{rel}, the relative power, can be set to a value that results in acceptable coil losses. Then the amplitudes of the currents $\hat{I}_x$ and $\hat{I}_z$ can be calculated from H and TH.

4.1.5 Results

The parametric search starts with varying both the longitudinally magnetized magnet size HB (side magnets) and the width of the conductor bundle TH using the C++ program. The C++ data was loaded into Matlab to visualize the results. The Matlab scripts can be found in appendix B and the results can be seen in figures 4.3 and 4.4. Since the calculation involves two coils instead of the four coils required to control all three DoFs, the acceleration was calculated for half the translator mass.

These figures show that maximum acceleration occurs for a longitudinally magnetized magnet size HB of 8 to 9 mm and a conductor bundle width TH of 12.5 mm. The results for minimum ripple are a little different. The minimum ripple

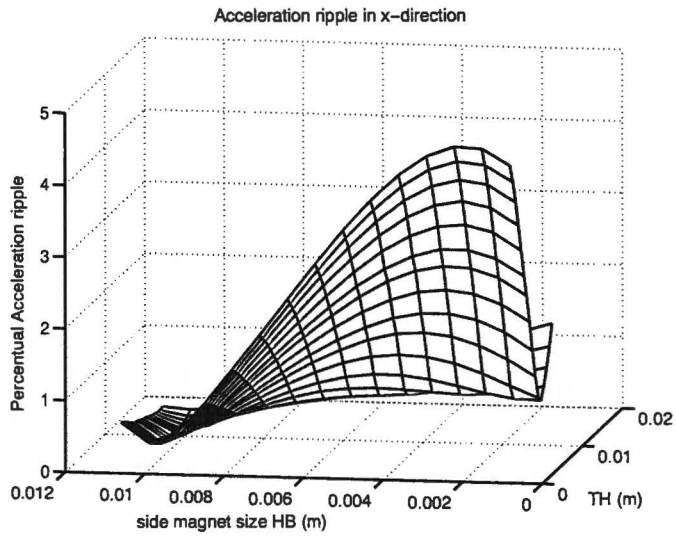

Figure 4.4. *Ripple on acceleration of the 3-DoF actuator as function of longitudinally magnetized magnet size and conductor bundle width*

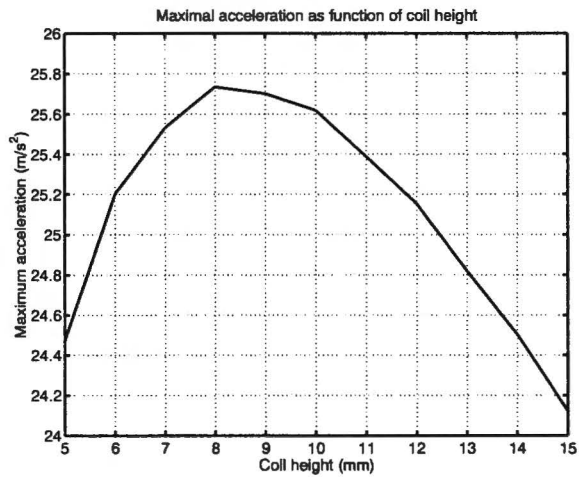

Figure 4.5. *Maximum acceleration in* x*-direction as function of the height of the coil*

occurs for a longitudinally magnetized magnet size of 10 mm and a conductor bundle width of 8 to 11 mm. Since a larger coil will give more options for fitting different wire sizes, it is best to choose a wide conductor bundle. Therefore, the selected values are a longitudinally magnetized magnet size of 10 mm and a conductor bundle width of 11 mm. The maximum acceleration in z-direction, as well as the minimum ripple in this direction, show the same behavior as the acceleration in x-direction.

The next step is to optimize the height H of the coil. The influence of this

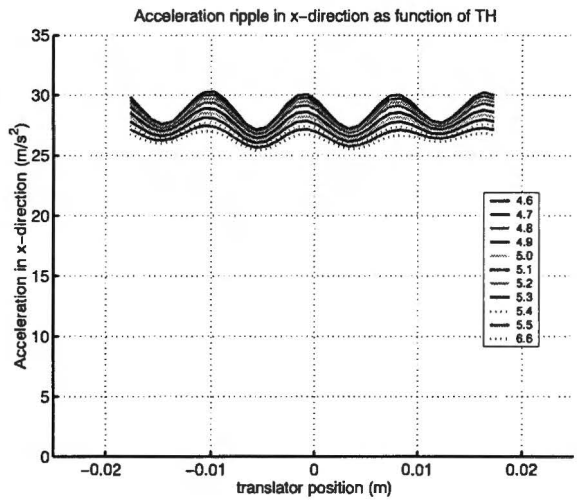

Figure 4.6. *Acceleration of the 3-DoF actuator as function of conductor bundle width*

parameter is smaller than that of the conductor bundle width, as is shown in figure 4.5. The optimal point was found at a height of 8 mm.

Another parameter that influences the results is the fillet radius of the coil windings. In the first case, the coil end was totally round. This means the fillet radius is equal to half the coil width. However, the force this configuration produces is less than the force you would get when the fillet radius is minimal. The disadvantage of a small fillet radius is that it might cause problems during production, as the sharp edges of the production tool can damage the wire insulation in the corners.

Separately, the influence of the spacing of the conductor bundles is analyzed. This means that the bundle centers are no longer 1 τ_m (translator pole pitch) apart. It turned out that this decreases the force ripple significantly: the larger the bundle, the lower the ripple. This is shown in figure 4.6. Each line represents a certain width of the bundle, varying from 4.6 to 6.6 mm.

As a final step, this configuration is checked by the finite element model in Flux 3D. Therefore, the force results from C++ (based on the Lorentz method) are compared to the results from the FEM model, both by the Lorentz method and by the Virtual Work method. Only one fourth of a cycle (period) is calculated, because the rest is symmetrical. This shows that both Lorentz method calculations return the same waveform, but can have an offset of less than 3 percent, which is acceptable. The difference between the FEM Virtual Work and the C++ Lorentz method results is a little larger. Moreover, the Virtual Work results show a ripple. This is probably caused by the fact that the geometry is very hard to mesh. Virtual Work requires a high element density around the magnet array and the coils. Among other things, the number of elements could not be higher because it reached the software limit. Therefore, it is understandable that this method is less accurate.

All calculated data can be found in appendix D. Figures 4.7 to 4.9 show the force calculation results for the force components F_x, F_y and F_z when the coils are placed 1 mm below the magnet array . The y-component of the force is expected

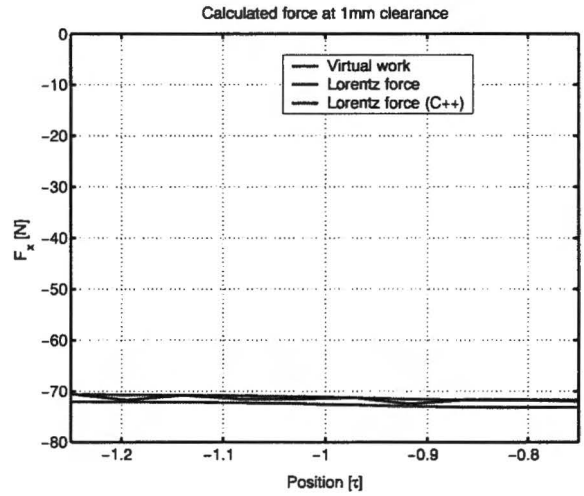

Figure 4.7. *Calculated values for force in x-direction*

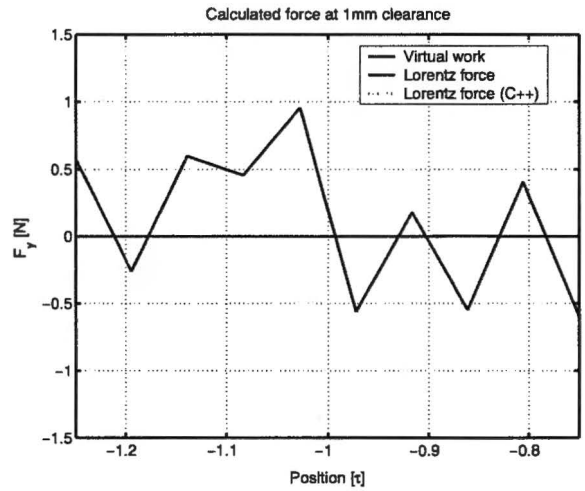

Figure 4.8. *Calculated values for force in y-direction*

to be zero. Both Lorentz method calculations indeed show that, but the Virtual Work method calculation is alternating around zero. However, both the x- and z-components from the Virtual Work method show a quite good agreement.

4.2 Number of turns

Calculating the number of turns requires a dynamic analysis of the actuator. Because this is outside of the scope of the M.Sc. project, but necessary for the design, this was performed by ir. J.W. Jansen and ir. C.M.M. van Lierop. Further details are described in [28].

The maximum specifications of the available power amplifiers are 100 V and

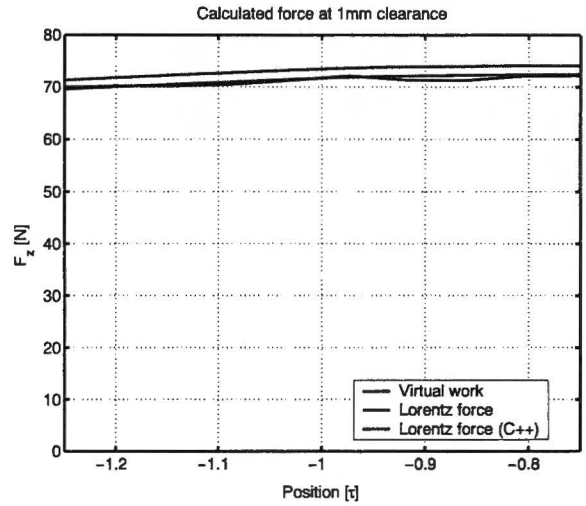

Figure 4.9. *Calculated values for force in z-direction*

16 A (peak values). Other specifications can be found in section 5.1.4. The number of turns per coil has to be adapted to these values. Therefore, the voltage across the coils (based on inductance and back-EMF) is calculated by an analytical model. The power amplifiers specifications result in the following optimization constraints:

$$V_{peak}(\mathbf{X}, N) \leq 100V \tag{4.18}$$

$$I_{peak}(\mathbf{X}, N) \leq 16A \tag{4.19}$$

$$I_{rms}(\mathbf{X}, N) \leq 10.6A \tag{4.20}$$

Based on experience, the number of turns is estimated to be within the following range:

$$100 < N < 400 \tag{4.21}$$

From the dimensions of the coils (such as TH and H), the estimated mass of the moving platform, the motion profile, and the specification of the power amplifiers, the number of turns per coil can be calculated using the voltage equation:

$$\mathbf{V} = R\mathbf{I} + \frac{d\vec{\psi}}{dt} \tag{4.22}$$

with

$$\mathbf{I} = K \begin{bmatrix} F_x \\ F_z \\ T_y \end{bmatrix} = K\mathbf{W} \tag{4.23}$$

therefore

$$\mathbf{V} = RK\mathbf{W} + \frac{\partial\vec{\psi}_0}{\partial x}\frac{dx}{dt} + \frac{\partial\vec{\psi}_0}{\partial z}\frac{dz}{dt} + LK\frac{d\mathbf{W}}{dt} + \frac{dx}{dt}L\frac{\partial K}{\partial x}\mathbf{W} + \frac{dz}{dt}L\frac{\partial K}{\partial z}\mathbf{W} \tag{4.24}$$

under the assumption that the pitch is zero (no rotation around y-axis).

The matrix K is the position dependent commutation matrix, which determines the current in the coils as function of the vector of reference forces F_x, F_Y and torque T_y, the wrench W. $\vec{\psi_0}$ is the total flux linkage in the coils, caused by the magnets, neglecting possible eddy current effects.

The calculations show that to meet the amplifier specifications, such as peak voltage, current output and impedance, the number of turns per coil should be around 300. The acceptable limits to keep the voltage and current within the specs are 250 to 350 turns.

4.3 Disturbances: eddy currents

Eddy currents are induced in the aluminium back plate of the stator by two sources: the current in the coils and the movement of the translator magnets. These eddy currents introduce damping of both the movement of the translator and the magnetic field of the coils.

Therefore, it would be advantageous to replace the aluminium by a material that has a low electrical conductivity. However, this material should also have a good heat conductivity to transport the heat which is produced in the coils. Certain ceramic materials have these properties. Eddy currents are described by the following equation:

$$\mathbf{J} = \sigma \cdot (\mathbf{E} + \mathbf{v} \times \mathbf{B}) \tag{4.25}$$

with $\mathbf{J}$ the current density, σ the conductivity of the material, $\mathbf{E}$ the electric field strength, $\mathbf{v}$ the speed vector and $\mathbf{B}$ the magnetic flux density.

The eddy currents induced by the magnets on the translator have been estimated by modelling this problem in Flux 2D. This model can be seen in figure 4.10. The model is rotated 90 degrees, because a translating air gap (the area surrounding the translator) in Flux 2D has to be oriented vertically. The translator moves at a speed of 2 m/s, while the thickness of the ceramic material in this picture is 10 mm. The air gap between translator and stator is 1 mm, and the coils are not energized.

The model was solved for seven values of thickness of the ceramic material. The resulting damping force on the translator can be seen in figure 4.11 Up to 10 mm thickness, the damping force drops very fast.

The other source of eddy currents is the current flowing through the coil conductors. This problem was also modelled in Flux 2D. Figure 4.12 a) shows the model with the eddy current density in the aluminium, with 1 mm of ceramic material, while in figure 4.12 b) the ceramic material is 10 mm thick.

The coils conduct a sinusoidal current with an amplitude of 3.5 A and a frequency of 100 Hz. The current phase is shifted 90 degrees per coil, because this would also be the case for normal operation. The results (that can be found in appendix D) show that the eddy current losses are halved when the thickness of the ceramic material is increased from 1 to 10 mm: at 1 mm, the total power is 46 W, while at 10 mm ceramic thickness, the total power drops to 23 W. Detailed values can be found in appendix D.

Properties of the ceramic material

The ideal ceramic material for the actuator should have a very low electrical conductivity, as well as a heat conductivity of the same magnitude as that of aluminium. The material that seems to be best for this purpose is aluminium nitride, although

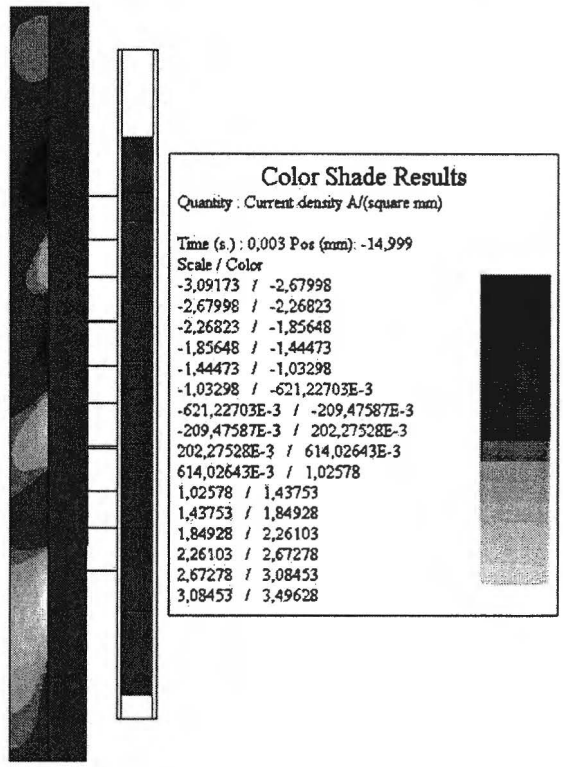

Figure 4.10. *Eddy current density in the aluminium back plate of the stator, calculated by Flux 2D at a speed of 2 m/s*

its very low expansion coefficient requires a flexible mounting to the aluminium back plate and the coils. The properties of this material and those of aluminium are shown in table 4.1.

		aluminium nitride	aluminium	
Density		3.30	2.70	g/cm^3
Resistivity (20 °C)	ρ	10^{14}	$2.67 \cdot 10^{-6}$	Ωcm
Thermal conductivity	k	180	237	W/mK
Expansion coefficient		4.6	~ 24	10^{-6} K
Max. use temperature	T_{max}	1000	~ 650	°C

Table 4.1. *Most important properties of AlN and Al*

4.4 Thermal analysis

Thermal analysis involves analyzing the heat flows in and around the actuator. Heat can be transported by three different mechanisms: conduction, convection and radiation [29]. Conduction is heat flow within a body or between two bodies

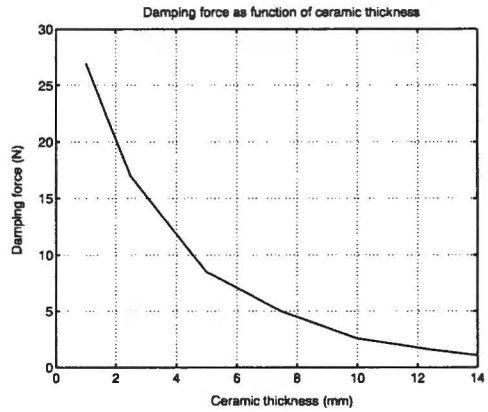

Figure 4.11. *Damping force on the translator as function of the thickness of the ceramic plate (translator speed: 2 m/s)*

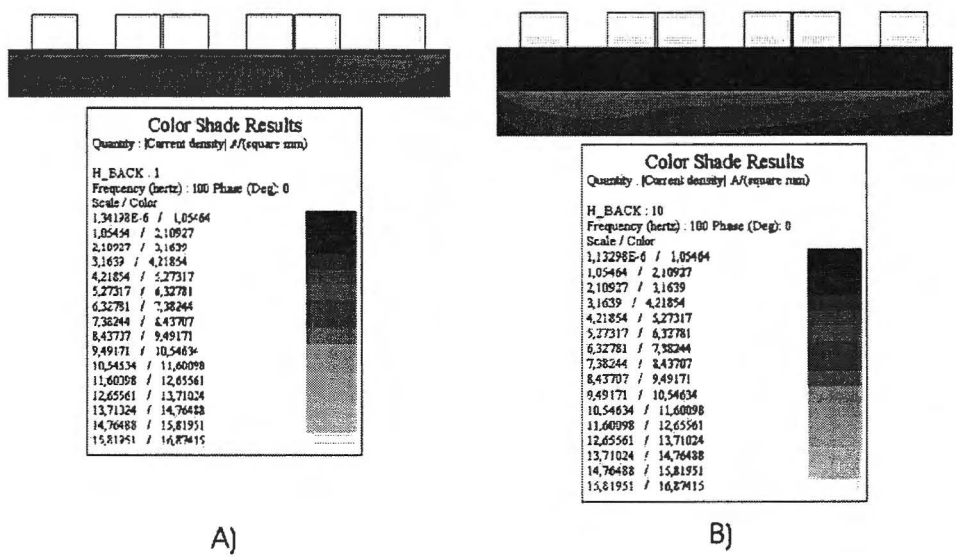

Figure 4.12. *Eddy current density in the aluminium back plate at a frequency of 100 Hz, calculated by Flux 2D for A) 1mm ceramic material and B) 10 mm ceramic material*

in contact. This flow depends on the thermal conductivity constant k of a material. The amount of heat that flows through the material (or from one material to another), the heat flow H_c, can then be described as:

$$H_c = \frac{dQ}{dt} = -kA\frac{dT_{abs}}{dx} \tag{4.26}$$

where Q is the heat flux, t is the time, A is the conductive area and T_{abs} is the absolute temperature. The thermal conductivity of aluminium is approximately 200 W/mK. That of air is only 0.024 W/mK when the air is not moving. The air

around the test-setup is moving, therefore convection occurs. Convection is the transfer of heat by mass motion of a fluid or gas. In air, this movement is caused by thermal expansion due to temperature differences. This process is called natural convection. Heat transfer due to convection is a very complex process. Therefore, it can not be described by a simple equation. It is however clear that heat current due to convection is directly proportional to the surface area of the "hot" material. This fact is used in the thermal model.

The third mechanism of heat transfer is radiation. This is heat transfer by electromagnetic waves, such as visible, infrared and ultraviolet light. Every object with a temperature that is higher than its surroundings emits energy in the form of radiation. As with convection, the rate of energy radiation is proportional to the surface area A. The rate also depends on the nature of the surface. This dependence is described by the emissivity e, a dimensionless number between 0 and 1. For a smooth copper surface, e is about 0.3. Furthermore, the radiation depends on the fundamental Stefan-Boltzmann constant $\sigma = 5.6705119 \times 10^{-8} W/m^2 \cdot K^4$. Knowing this, the heat flow due to radiation can be defined as

$$H_c = Ae\sigma T^4 \tag{4.27}$$

In the actuator under design, the coils are the main heat sources. They heat up when they are energized due to the resistance of the copper. This heat has to be conducted to the outside of the system. From the surface, the heat will be transported by natural convection and radiation. This total heat flow is estimated by a 2D FEM analysis in Flux 2D. The models (showing the temperature iso values at steady state) are shown in figure 4.13. They do not include the translator, because there is a layer of air between the stator and the moving part, which has a comparatively low heat transfer coefficient. A minor heat source is the presence of eddy currents in the back plate of the stator. This minor source is not modelled.

As can be seen from the model, there is a small layer present between the ceramic material and the aluminium back plate. This layer represents the glue between the surfaces of the materials, because this has a low heat transfer coefficient. A similar layer is present between the coils and the ceramic material, because there is a thin layer of resin in between. The space in between the coils is filled with a heat-conducting resin. One of the models also includes the supporting aluminium plate, because this has a large heat capacity and a large area for radiation and convection. The plate is not placed in the real direction, because this would require a 3D-model.

The model is based on the real test-setup. To be able to obtain a fast estimation, only three coils are modelled instead of ten. Because the cooling area increases linearly with the number of coils, this should give a good estimation of the result. The heat source in the top coil was set to 75 W per conductor bundle. The middle coil has no source, while the lower coil has a source of 5 W per conductor bundle. These values are based on a worst case value of the coil current, which occurs when the translator is levitated in one position, supported by two coils (the top and lower one).

Both the model with support and without support are used for a transient simulation. The model without support reaches steady state in approximately 2700 seconds (45 minutes). The temperature of the upper coil has then increased to 207 °C. This is higher than the temperature limit of the coils, which is 170 °C. Luckily, the influence of the support plate is evident: this model reaches steady state in 5400

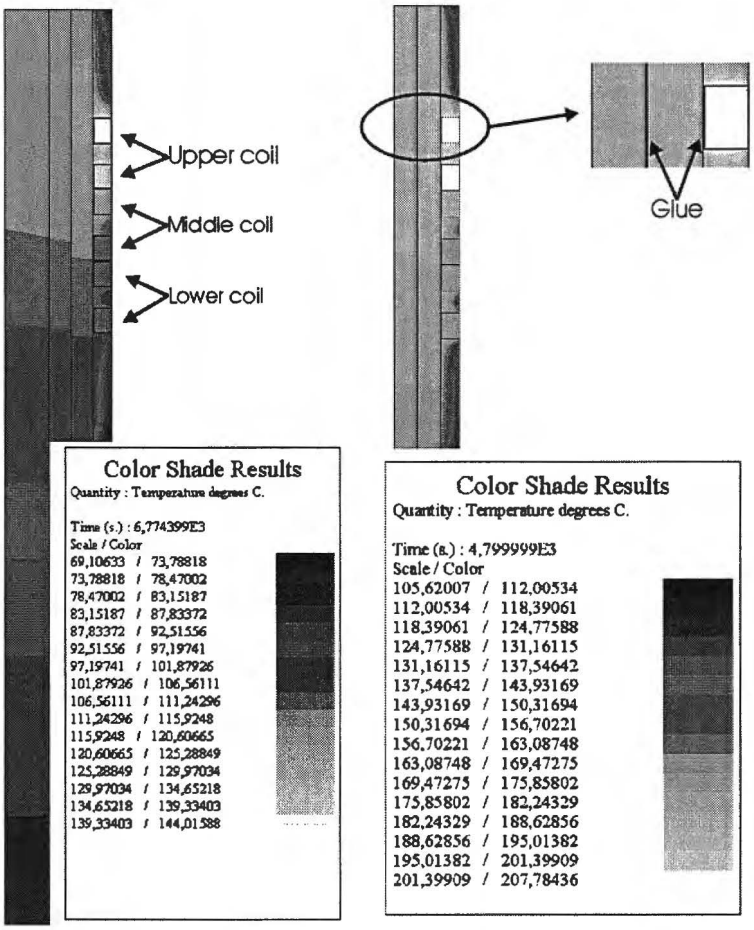

Figure 4.13. *Thermal models in Flux 2D in steady state (with and without the support plate)*

seconds (90 minutes). The upper coil temperature is then 145 °C. The transient responses of the two models are shown in figures 4.14 and 4.15.

The calculated steady-state temperature of 145 °C is below the maximum temperature of the coils. This means that the actuator does not require extra cooling. However, heat transfer coefficients between the different materials in the real setup are very hard to estimate. Therefore, temperature sensors will be mounted to the surface of every coil to protect the setup from overheating. Moreover, the back plate of the stator will be constructed in such a way that it is possible to mount a water cooling system to this plate.

Furthermore, the design is mainly meant for identification. This means the operation time will be around 10 minutes per experiment. Even at the worst case scenario, the upper coil temperature will remain less than 100 °C, which is within all material limits.

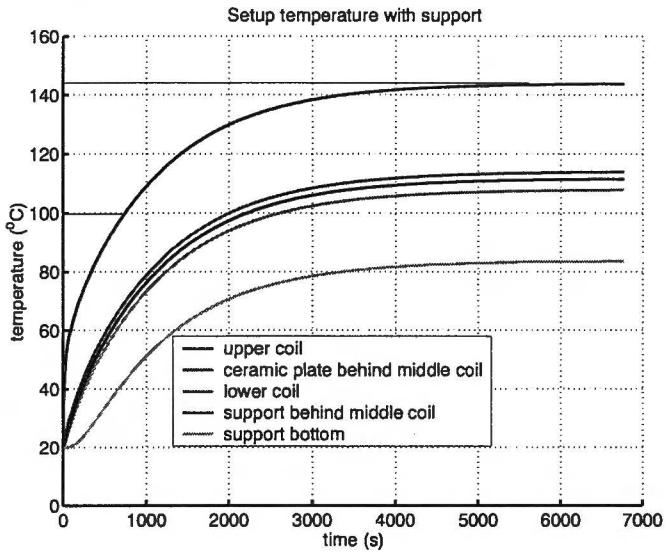

Figure 4.14. *Temperature of the setup for the model with the support*

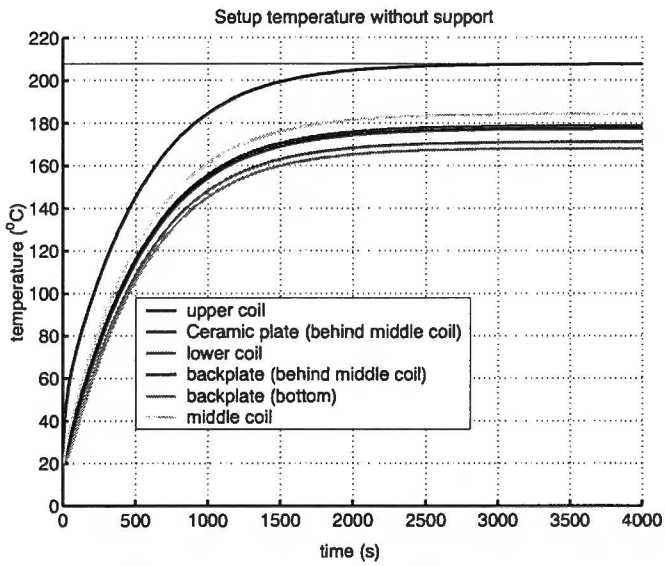

Figure 4.15. *Temperature of the setup for the model without the support*

4.5 Conclusion: final design

The initial electromagnetic design was optimized for both most efficient acceleration in x- and z-directions and minimum acceleration ripple in these directions, based on 20x20x8 mm sized pole magnets. Furthermore, the number of turns per coil was adapted to fit the amplifier specifications. This resulted in the following sizes and numbers:

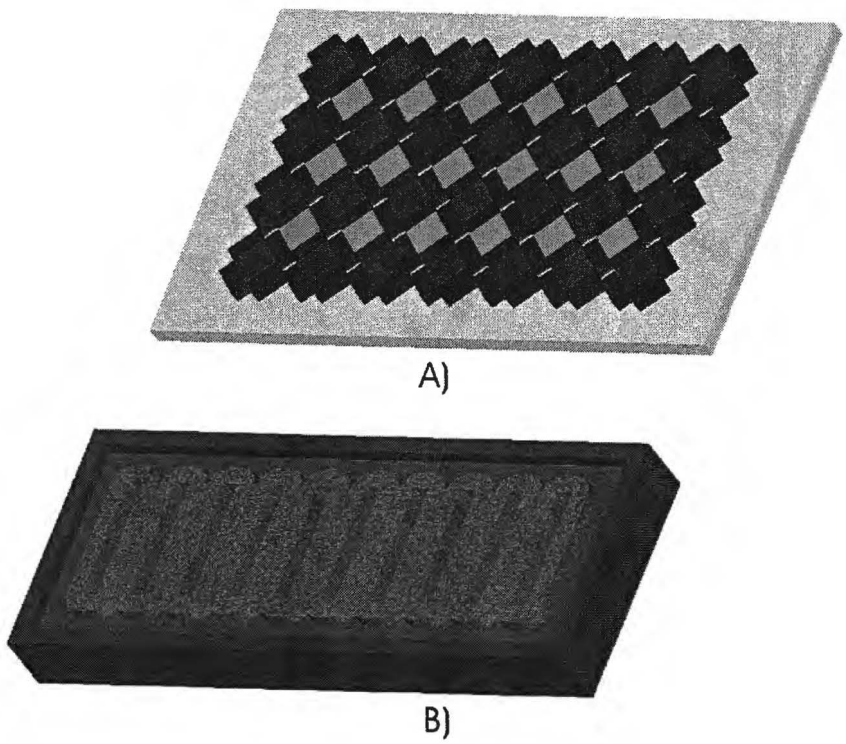

Figure 4.16. *The final design A) Translator B) Stator*

- Longitudinally magnetized magnet width HB: 10 mm,
- Coil conductor bundle width TH: 11 mm,
- Translator pole pitch τ_m: 21.21 mm,
- Coil height H: 8 mm,
- Number of turns per coil N: $\sim$ 300 (final number is determined later, see section 5.1.3).

The back plates of both stator and translator are assumed to be made of aluminium with a thickness of 10 mm. Since aluminium is a good electrical conductor, eddy currents will be induced in the plate, resulting in damping of the magnetic field and a damping force on the translator. Therefore, a 10 mm thick ceramic plate will be positioned between the coils and the stator back plate. Figure 4.16 shows the resulting sizes of the setup.

Finally, thermal analysis showed that this setup can operate without extra cooling. However, precautions will be made to protect the setup from overheating.

Chapter 5

Realization & experiment

5.1 Realization of the test-setup

5.1.1 H-drive

Figure 5.1 shows a so called "H-drive". This is an actuator that can move in x- and y-directions and can also rotate a small angle around the z-axis. It consists of two parallel linear motors (the y-motors) with one linear motor perpendicular to these two, which is the x-motor. The coupling between the x-beam and y-motors is not stiff, so that a small offset in y-position is possible, resulting in the rotation around the z-axis.

This drive is used to support the 3-DoF linear actuator. To be able to use all three DoFs of the H-drive, the linear actuator will be placed on its side, with the translator connected to the x-motor. In other words, the y-motors are coupled to the z movement of the linear actuator. The x-motor is then coupled to the x-movement of the actuator. Finally, the rotation of the actuator around the y-axis can be performed by the z-axis rotation of the H-drive. In order to test the levitation capabilities of the linear actuator, the H-drive should create artificial gravity. This creates the possibility to test with any value for the gravity, for instance to determine the maximum levitation power of the 3-DoF actuator.

Besides supporting the translator in its three DoFs, the H-drive also fixes the additional three DoFs of the actuator. Therefore, the control complexity during the implementation and the test phase of the controller is decreased. In addition, the H-drive can be used both for position measurements and as a safety layer to prevent collisions of the magnet array with the stator coils. Nevertheless, the rigid connection between the H-drive and the pre-prototype causes a change in the dynamic behavior of the actuator. In order to compensate for the additional and therefore unwanted dynamics, the H-drive has to be controlled using force-feedback. This control strategy slightly resembles haptic control, which is mainly used in minimal invasive surgery.

The control of the H-drive and the 3-DoF actuator is outside of the scope of this thesis, but is required to perform measurements. The control layout, as is displayed in figure 5.2 is determined by ir. C.M.M. van Lierop and is described in [28]. Here, the commutation algorithm is the position dependent commutation matrix K, $C_{actuator}$ is the pre-prototype controller, $C_{H-drive}$ is the "haptic" controller, *dq0*

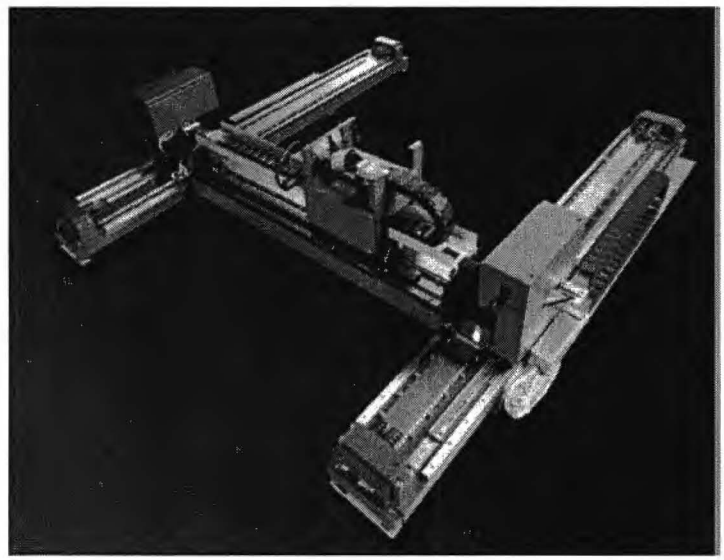

Figure 5.1. *The H-drive*

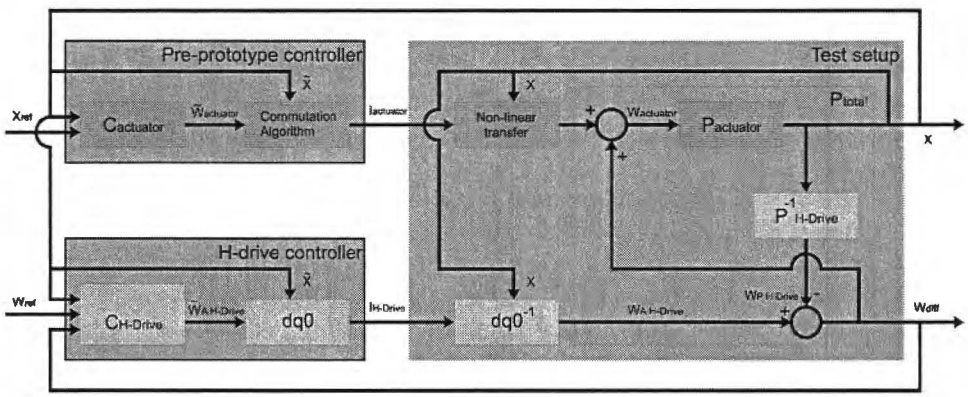

Figure 5.2. *Block scheme of the "haptic" control of the H-drive*

is the transformation from the controller output to the motor currents, $P_{actuator}$ is the pre-prototype transfer-function, $P^{-1}_{H-drive}$ is the inverse of the H-drive transfer-function, X represents the position vector and W_{dif} is the measured wrench (the vector of force- and torque-components) between the H-drive and the translator.

5.1.2 Translator

The magnets that are used in the optimization process are of the BM35 type from Bakker Magnetics. When the magnets were ordered, it turned out that it was relatively cheap to order a higher quality magnet (having a higher remanence and a higher temperature limit). Therefore, the final magnets are of BM38SH quality. The specifications of this permanent magnet material can be found in appendix C. The magnet sizes remain the same: 20 mm by 20 mm by 8 mm for the pole

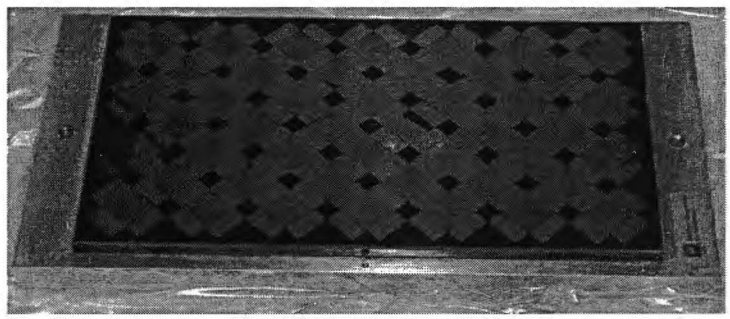

Figure 5.3. *The translator (bottom view)*

magnets and 20 mm by 8 mm by 10 mm for the longitudinally magnetized magnets. These magnets do not have to be coated, because the material has a special rust protection.

The magnets are glued to the aluminium back plate by Bakker Magnetics. It turned out that the magnets on the sides are very difficult to glue because of the repulsive forces between the pole magnets and the longitudinally magnetized magnets. Therefore, the magnets are placed in a resin and are ground afterwards to get a flat surface, as can be seen in figure 5.3. The thickness of the back plate as used in the calculations is 10 mm. However, after consulting Bakker Magnetics, the thickness is increased to 15 mm to have a higher stiffness. The total mass of the translator is now 5.635 kg, of which 3.048 kg is aluminium.

5.1.3 Stator

Coils

The 10 coils for the stator part are manufactured by Tecnotion BV from Almelo. The exact sizes (as stated in section 4.5) were given to them, but the number of turns per coil was set by Tecnotion, (within a range of 250 to 350) to be able to use a wire diameter that fits the sizes best. The sizes of the final coil, which has 348 turns, can be seen in figure 5.4. A picture of the coil is placed in appendix E. The copper diameter of the wire is 0.45 mm. This wire has a resistance of 0.1 Ohm per meter. The coil is wound according to the orthocyclic principle, which means that wires are placed exactly in between the wires of the previous layer. This results in a higher fill factor (copper area divided by total area). The cross-over point is placed at one of the short sides of the coil.

The coils are glued to the ceramic plate by a two-component glue. Positioning of the coils is done by means of a separate alignment tool, which is removed afterwards. To ensure both a stable construction and a good heat conduction from the coils, the area around the coils is filled with a resin, type Stycast. This is also done at Tecnotion. This resin is chosen because it has a thermal conductivity of 0.6 W/mK and because it is flexible, since the expansion coefficients of copper and aluminium nitride are very different.

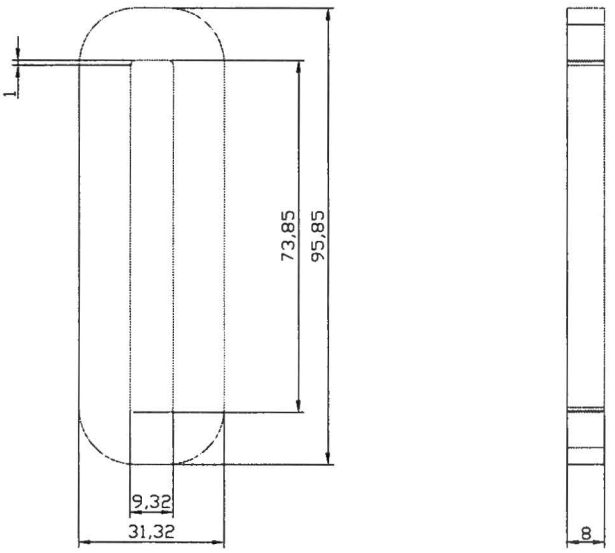

Figure 5.4. *Dimensions of the coil*

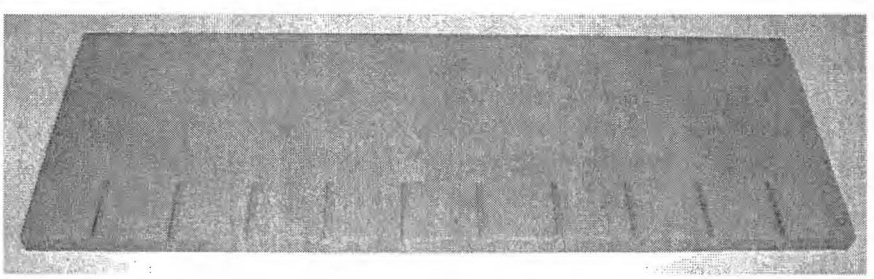

Figure 5.5. *The aluminium nitrite plate*

Ceramics

The aluminium nitrite ceramic plate, as already mentioned in section 4.3, is manufactured by Gimex, Geldermalsen. This material was chosen because of the high thermal conductivity (180 W/mK) and the very high electrical resistivity (10^{14} Ωcm). The dimensions are 350 mm by 120 mm by 10 mm. As can be seen in figure 5.5, grooves have been cut out of the plate. These are required to pass the inside wire of the coils to the outside of the stator. The wires from the temperature sensors (see section 5.2.3) also pass through these grooves. The exact sizes can be found in the drawing in appendix E.

Aluminium stator frame

The GTD of the TU/e has manufactured an aluminium back plate with removable edges to form a frame. This is used to hold the ceramic plate and the coils in place. After the stator is filled with resin (Stycast), the edges are removed and the ceramic plate is glued to the aluminium back plate. This plate has a thickness of 20 mm.

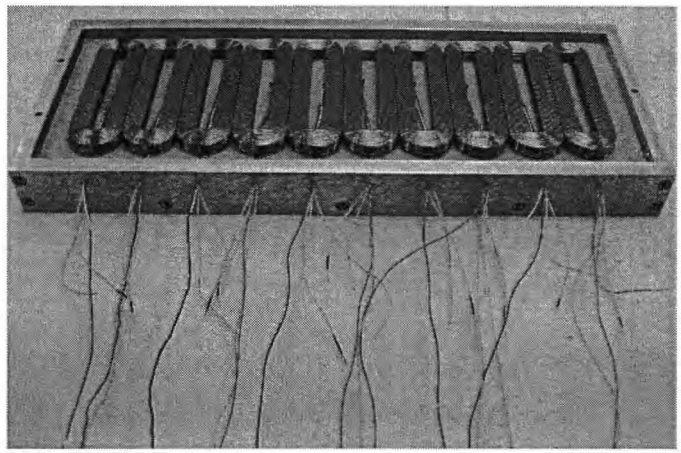

Figure 5.6. *The aluminium stator frame*

Figure 5.6 shows the frame with the ceramic plate, the coils and the temperature sensors in place, the resin was not yet applied. A picture of the stator filled with resin can be found in appendix E

5.1.4 Power amplifiers

The power converters are current amplifiers (PADC 100/16), which are designed and manufactured by Prodrive. The amplifiers are donated by ASML and Prodrive and they are all tested and updated to the latest version by Prodrive. The amplifiers require a high power DC input, supplied by four PSDC 59/22 supplies (also from Prodrive). Moreover, a 5 V and 15 V input is required. These are supplied by two Delta elektronica low voltage power supplies. The specifications of the power amplifiers can be found in table 5.1. A picture of the amplifiers can be found in appendix E.

Power Output	specification	dimension	comment
Operational output voltage range	-100 to + 100	V	differential
Operational output current range	-16.4 to +16.4	A	differential
Absolute voltage maximum	$< 60, > -60$	V	to ground

Table 5.1. *Properties of the Power amplifier output*

5.1.5 Supports

A support is needed to mount the stator on the same level as the x-motor of the H-drive. The final design and manufacturing of this part is done by the GTD of the TU/e. A picture of the support can be found in appendix E. The support is made of aluminium with a thickness of 20 mm. It is mounted to the baseplate of the H-drive. The part where the stator has to be mounted is equipped with elongated holes, to be able to position the stator exactly and compensate for alignment errors.

Furthermore, the translator has to be mounted to the x-motor of the H-drive, while force sensors have to be placed in between. The GTD also manufactured an aluminium adapter for this, which fits the mounting holes on the motor, as can be seen in appendix E.

5.2 Sensors

Sensors are needed in the test setup, not only for measurement purposes, but also to protect the test-setup. The different sensors are described in the next sections.

5.2.1 Force sensors

Force sensors are required to measure the force between the translator and the x-motor of the H-drive, both for measurement of the force produced by the actuator and for control in force-feedback mode. The sensors are mounted in between the translator and the H-drive by means of a stainless steel bolt. This bolt supplies the required preload on the sensor. The sensors are 3-DoF, measuring the force in x- and z- directions (y-direction is not used). By placing two sensors, it is also possible to measure the torque T_y.

The available sensors are made by Kistler (see appendix G). The sensors have a range of 2.5 kN (at a standard preload of 25 kN). They are of the piezoelectric type. This means a charge flow can be measured when there is a changing force on the sensors. In other words, these sensors cannot measure absolute forces, but only the change in force. This is not a problem for identification. However, if the actuator is to be used in motoring mode, the absolute force has to be known in order to operate the H-drive in slave mode. Then, another type of sensor would be necessary. A picture of the placement of the sensors can be found in appendix G.

5.2.2 Position sensors

For identification, it is important to know the exact position of the translator, relative to the stator. The position sensors of the H-drive are used for this purpose. These are Heidenhain encoder rulers of the LIDA 201 type, that have a micrometer accuracy.

As a backup for the encoders, to protect the setup, a proximity sensor can be placed on the actuator. This will stop the movement of the H-drive if the distance between translator and stator becomes to small. However, due to time constraints, this sensor is not yet implemented.

5.2.3 Temperature sensors

Thermal analysis is a difficult problem, as small changes in the model can result large differences in the resulting temperatures. Therefore, it is not entirely certain that the temperature will stay within limits for all operation modes. To prevent overheating, temperature sensors are placed on all ten coils. The sensors are located in the center of the coil, glued to the inner conductors.

The sensors that are used are silicon temperature depended resistors with a temperature range of -50 °C to 150 °C, type KTY 21-6. These are recommended by Tecnotion. The resistance of such a sensor increases linearly with temperature. Details can be found in appendix G.

All sensor outputs are connected to an Agilent scanner (see appendix G), which will give an alarm when one of the sensor resistances is above a certain value. The temperature limit is set to 100 °C.

5.3 Control & data acquisition

The control of both the H-drive and the 3-DoF actuator is done by a dSpace system. This modular system can be adapted to the requirements of the experiment by adding input- or output cards with analog or digital inputs. Details of the system can be found in appendix G.

The dSpace system is also used to acquire the data from the force-, position and temperature sensors, as well as the voltages across and currents through the coils.

5.4 Transfer function of the coils

The resistance of the coil can be approximated by taking the average length of a winding and multiplying this by the number of turns and the wire resistance per meter. The average length is derived from the coil sizes and is 210.3 mm. The number of turns per coil is 348. At a wire resistance of 0.1 Ω/m, this results in a total coil resistance of 7.32 Ω.

The resistance of all 10 coils is measured with an Agilent scanner (see appendix G). The average resistance is 6.24 Ohm. The measurement data can be found in appendix F. This means the calculated value is too high, which can be caused by the approximation of taking the average length or a different value of typical resistance of the wire.

The inductance of the coil is calculated with Flux 3D to be 6.86 H. Measuring the inductance by using a measurement bridge (see appendix G) (the coil was not placed on the stator) results in a value of 7.05 H, which is only 2 % higher.

The mutual inductance is also calculated with Flux 3D. For two neighboring coils, the mutual inductance is -0.83 H. This mutual inductance is not yet measured.

5.5 Force-position

To measure the position-dependent force, it would be best to use the H-drive to position the translator in x- and z-directions. However, the force sensors show nonlinear behavior, making it difficult to get accurate force readings in steady state. Therefore, the H-drive is used to move the translator at a low speed of 2 cm/s, while the forces are recorded constantly by the dSpace system. Even in this case, the charge amplifier that is connected to the force sensors has an increasing offset, and the signal shows some other disturbances. These are corrected by subtracting a reference measurement (measured when there was no current in the coils) from the actual measurements. This is done off-line in Matlab.

The recorded forces show a lot of "noise". These signals come from higher dynamic modes of the H-drive and the translator. Since the control bandwidth of the H-drive controller is 50 Hz, signals with a higher frequency are not suppressed. The frequency of the measured signal is about 0.5 Hz, therefore it is acceptable to suppress frequencies higher than 25 Hz by a filter. The filtering was also performed off-line in Matlab, using a non-causal filtering method to obtain zero phase shift.

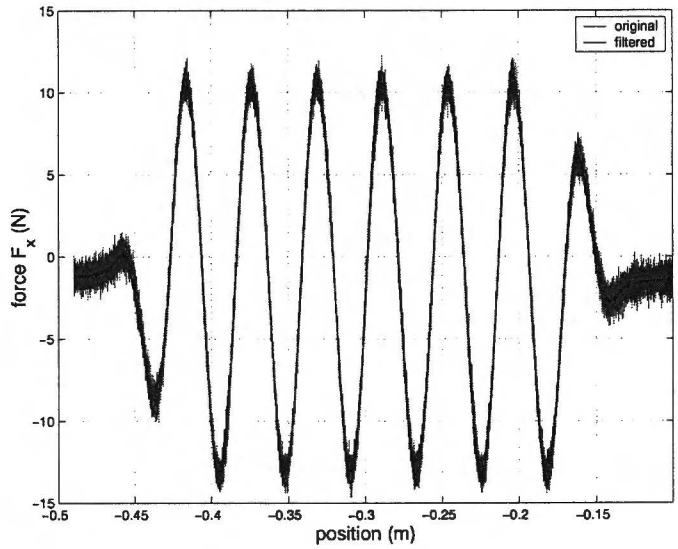

Figure 5.7. *Measured signal, original and filtered*

The Matlab code that is used can be found in appendix B. The influence of the filter is illustrated in figure 5.7, where both the original and the filtered signal of F_x are displayed.

5.5.1 Results

A constant current of 1 A is applied to one or more coils during measurement. First, a measurement with one energized coil is done. The force in x-direction is compared to simulations, as can be seen in figure 5.8. These results are in good agreement, even though the force measurement shows a small offset.

Figure 5.9 shows the measured forces for one active coil. The signals of the two sensors in z-direction are shown separately. From this it can be seen that the coil is first one the one side of the array, moving to the other side. If the two x-components are added, the waveform is similar to that of F_x, but shifted 90 degrees in phase, which is as expected.

An interesting measurement is shown in figure 5.10. Here, 2 coils are active, coil no. 1 and coil no. 3. These two coils are in the same relative position with respect to the magnet array, only the polarity of the magnetic field is opposite. Because both coils are conducting a DC current of 1 A, this means the forces on the coils should cancel out. The figure shows that this is indeed the case, but only when both coils are fully covered by the array and experience no edge effects. This can be seen immediately from F_x, which is approximately zero in the middle of the array. When the two F_z components are summed, the result is also zero in the middle of the array.

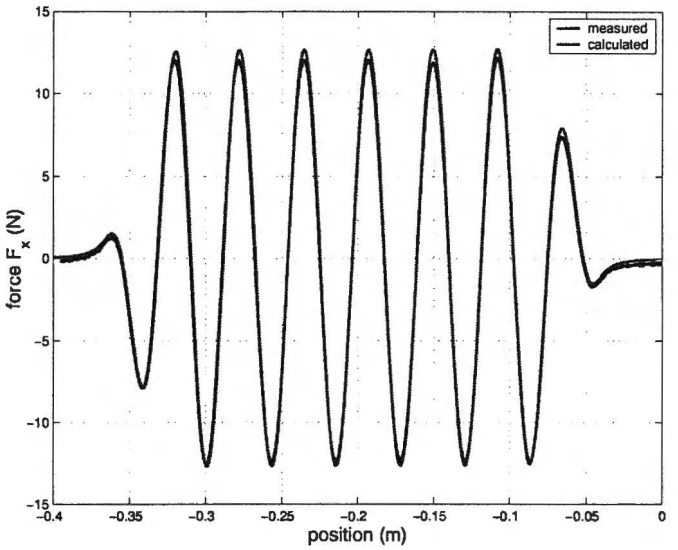

Figure 5.8. *Measured and calculated force*

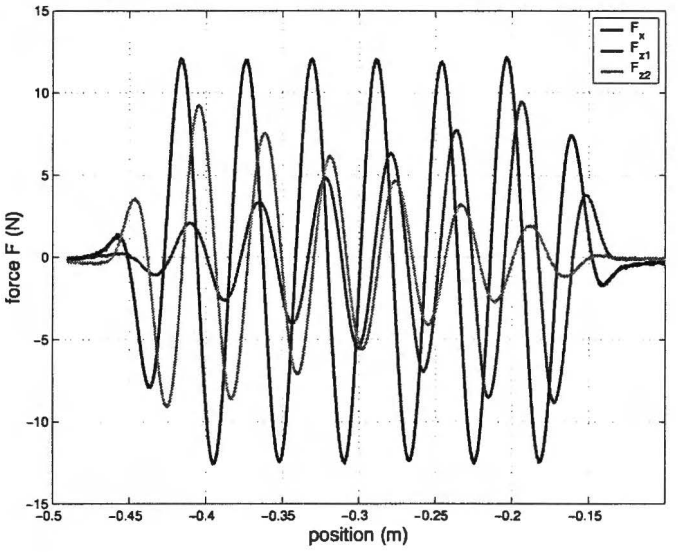

Figure 5.9. *Measured force for 1 active coil*

5.6 EMF

The EMF (ElectroMotive Force) can be measured as the induced voltage in a coil when the translator is moved. In this experiment, the H-drive acts as master and moves the translator at a constant speed of 0.5 m/s along the stator. This is done at three different distances: 1 mm, 2 mm and 3 mm. One of the ten coils was connected to a dSpace input via a 1 to 1 probe. The measurements are normalized to 1 m/s to be able to compare them to calculations.

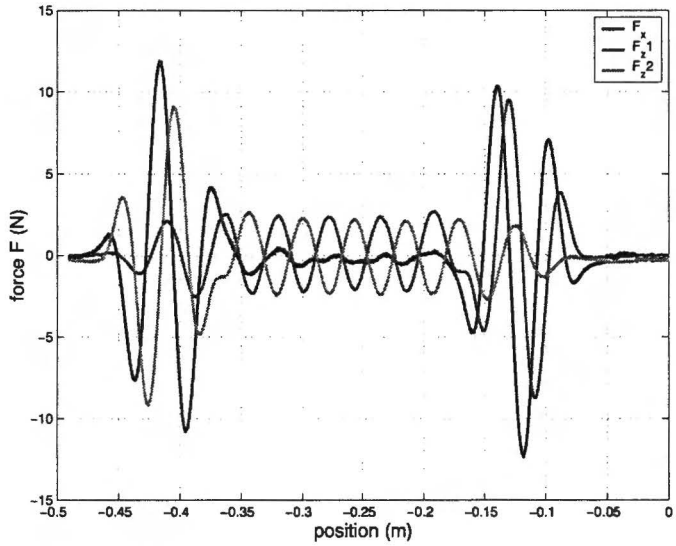

Figure 5.10. *Measured force for 2 active coils*

With the static models that are available, it is not possible to calculate EMF. However, it is possible to calculate force. When a constant current is applied, the force waveform should be the same as the EMF waveform (neglecting eddy currents in the back plate). Therefore, force- and EMF waveforms can be compared. These results are submitted to the IEEE IEMDC 2005 conference for publication.

5.6.1 Results (compared to simulations)

Figure 5.12 shows the measured EMF for an airgap of 1 mm at a speed of 1 m/s, as well as the force calculation for a DC current of 1 A in one coil. The results are in good agreement. Figure 5.11 then shows the measured EMF for air gap heights of 1, 2 and 3 mm. It is clear that the amplitude of the EMF decreases when the distance between stator coils and translator magnets is increased.

5.7 Conclusion

The force the stator produces on the translator has been measured for both a one-active coil and a two-active coils configuration. The results from one coil are compared to simulations, and they show good agreement. The small difference can be caused by a lot of factors, that should be identified later.

The EMF measurement also shows good agreement with the estimations. A first conclusion from this result is that the magnet array meets its specifications. However, some other factors are influencing the results, such as eddy currents in the back plate of the stator. These factors should be investigated.

More measurements are required to fully check the estimated forces with the measured forces and to identify the actuator. Because of time constraints, these measurements are not included in this thesis, but they will be performed in the near future, as part of the work of ir. J.W. Jansen and ir. C.M.M. van Lierop.

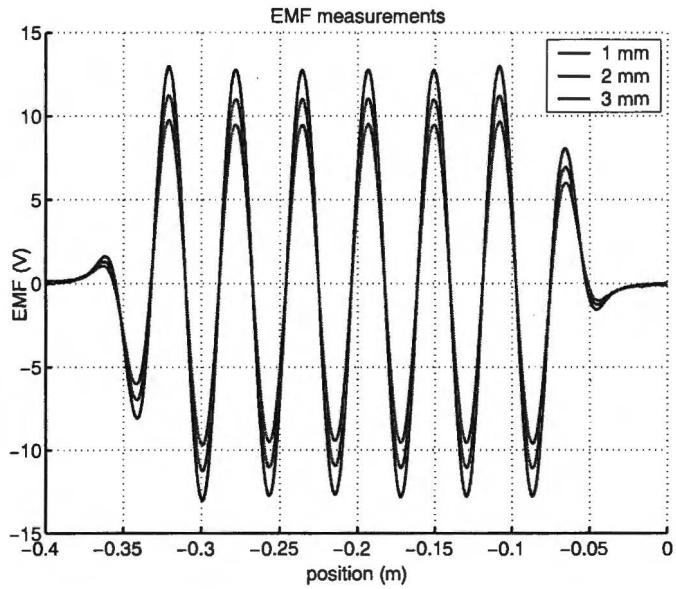

Figure 5.11. *Measured EMF for three airgap heights at 1 m/s*

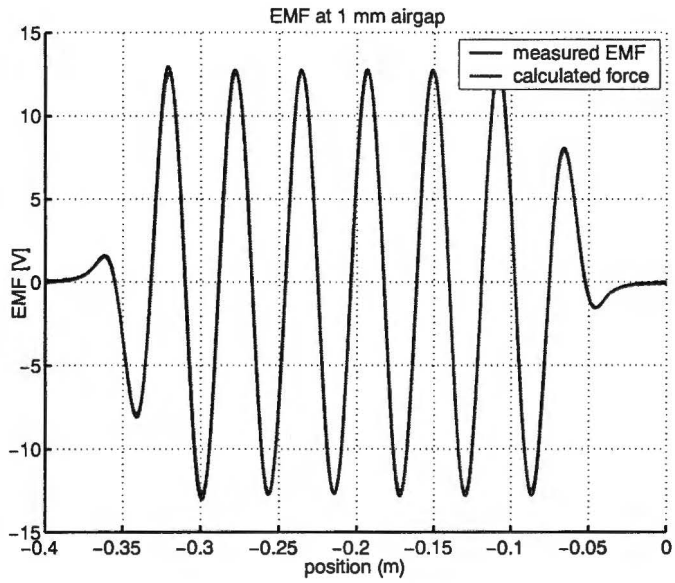

Figure 5.12. *Measured EMF compared to calculated force*

Chapter 6

Conclusions and recommendations

6.1 Conclusions

- The relevant literature is searched for permanent magnet electrical actuators, both linear and planar. Because most linear actuators do not include magnetic levitation, few topologies are comparable to the 3-DoF actuator under design. Moreover, few performance indexes are available of designs that are comparable.
- The explicit investigation of rectangular variation in Halbach magnet arrays is done. By the implementation of the design principles of the 3-DoF actuator, the unique specifications of the eventual 6-DoF actuator are met, because of the 2D magnet array structure.
- The actuator structure is optimized electromagnetically for maximum acceleration in x- and z-directions and minimum acceleration ripple in those directions. The optimization was done using a parametric search, within constraints resulting from available magnet size, amplifiers and measurement setup. The tools for this parametric search are based on C++ code.
- A thermal analysis is performed on the design, showing that it can operate without additional cooling. However, thermal sensors are installed in the test-setup to protect it from overheating.
- The performance of the final design is checked by Finite Element Method Calculations in Flux 3D.
- It is shown that two neighboring stator coils are capable of both suspending and propelling the translator. To control the torque T_y as well, four neighboring coils will be required.
- The 3-DoF actuator is realized and tested in the laboratory of the EPE group. A so-called H-drive is used to support the actuator. The measured behavior is comparable to the calculations.
- The aluminium support plate plays an important role in the thermal behavior of the setup. This is caused by its large area and heat capacitance. Without this plate, simulations show that the coils may be overheated within 10 minutes.

6.2 Recommendations

- The thermal analysis is only performed by FEM simulations in Flux 2D. Because there are few references to check the results, the accuracy of the results is unknown. A more thorough analysis (possibly in 3D FEM) could be performed to achieve results that are more reliable.
- For new design assignments, it is important to contact the manufacturers of the parts in a very early state, both to get a feeling about problems that might occur during manufacturing, and to inform about delivery times. This process will consume a lot of time.
- Optimization of the sizes of the planar motor should be based on an analysis of the forces in every position of the translator.
- Measurements of the 3-DoF test setup should be continued, in order to get more experience with the setup, which can be useful for the future measurements on the planar actuator.
- The influence of the presence of the ceramic plate on coil inductance, eddy currents and translator damping forces should be checked.
- The magnet array (i.e. its space harmonic distribution) has a significant influence on the force and stator losses. The consequences of this for the 6-DoF actuator should be investigated.
- The translator magnet array produces a strong magnetic field. The influence of this field on the environment of the actuator should be investigated.

Bibliography

[1] K. Halbach, "Design of permanent multipole magnets with oriented rare earth cobalt material," *Nuclear inst. and methods*, vol. 169, no. 1, pp. 1–10, Feb 1980.

[2] S. Earnshaw, "On the nature of the molecular forces which regulate the constitution of the luminiferous ether," *Trans. Camb. Phil. Soc.*, vol. 7, pp. 97–112, 1842.

[3] H. J. Düll, "Long stator linear motor without iron," U.S. Patent 4,303,017, 1979.

[4] M. Morishita, T. Azukizawa, S. Kanda, N. Tamura, and T. Yokoyama, "A new maglev system for magnetically levitated carrier system," *IEEE Trans. Vehicular Tech.*, vol. 38, no. 4, pp. 230–236, 1989.

[5] I. Y. A. Wang, S. H. Li, and I. Busch-Vishniac, "A magnetic levitation transport path," *IEEE Trans. Semicond. manufact.*, vol. 4, no. 2, pp. 145–154, 1991.

[6] K. Yoshida, A. Fuji, and H. Takami, "Pass-through-section experiment in mass-reduced-mode of controlled-repulsive pm lsm maglev vehicle by new dtc method," in *Proceedings of the Power Conversion Conference Osaka 2002*, no. 2, Osaka, Japan, Apr 2002, pp. 867–872.

[7] J. W. Jansen, "Preliminary investigation of a planar motor with a moving magnet configuration and with six degrees of freedom," Master's thesis, Eindhoven University of Technology, Eindhoven, The Netherlands, Jun 2003.

[8] B. A. Sawyer, "Magnetic positioning device," U.S. Patent 3,376,578, April 2 1968.

[9] E. R. Pelta, "Two-axis sawyer motor for motion systems," *IEEE Control systems magazine*, vol. 7, no. 5, pp. 20–24, 1987.

[10] A. F. flores Filho, A. A. Susin, and M. A. da Silveira, "Development of a novel planar actuator," in *Proc. of the Ninth International Conference on Electrical Machines and Drives*, no. 468, Canterbury, UK, September 1999, pp. 268–271.

[11] D. Ebihara, T. Watanobe, and M. Watada, "Characteristic analysis of surface motor," *IEEE Trans. Magn.*, vol. 28, no. 5, pp. 3033–3035, 1992.

[12] D. A. Markle, "Magnetically-positioned x-y stage having six degrees of freedom," U.S. Patent 5,886,432, 1999.

[13] H.-S. Cho and H.-K. Yung, "Analysis and design of synchronous permanent-magnet planar motors," *IEEE Trans. Energy conv.*, vol. 17, no. 4, pp. 492–499, 2002.

[14] T. Asakawa, "Two-dimensional precise positioning device for use in a semiconductor manufacturing apparatus," U.S. Patent 4,535,278, August 13, 1985.

[15] T. Teng, T. Ueda, S. Makinouchi, and B. Yuan, "Moving magnet type planar motor control," in *Proceedings of the International Conference on Positioning Technology*, Hamamatsu, Japan, June 2004, pp. 203–208.

[16] J. Tsuchiya and G. Kimura, "The excitation patterns and torque characteristic of moving-magnet-type surface motor," in *Proceedings of the European Power Electronics Conference 2003 (EPE 2003)*, Toulouse, France, Sep 2003, pp. 1–7.

[17] J. C. Compter and P. C. M. Frissen, "Displacement device," European Patent WO 01/18944, 2001.

[18] A. J. Hazelton, M. B. Binnard, and J. M. Gery, "Electric motors and positioning devices having moving magnet arrays and six degrees of freedom," US Patent 6,208,045, Mar. 27, 2001.

[19] M. Binnard, "Planar motor with linear coil arrays," US Patent 6,445,093, Sep. 3, 2002.

[20] J. Jin, *The Finite Element Method in Electromagnetics.* New York, USA: John Wiley & sons, inc., 2002.

[21] J. Jackson, *Classical Electrodynamics, 2nd edition.* New York, US: John Wiley and Sons, 1962.

[22] W. J. Kim, "High-precision planar magnetic levitation," Ph.D. dissertation, Massachusetts Institute of Technology, Cambridge, USA, Jun 1997.

[23] J. P. Yonnet and G. Akoun, "3D analytical calculation of the forces exerted between two cuboidal magnets," *IEEE Trans. Magn.*, vol. 20, no. 5, pp. 1962–1964, 1984.

[24] J. W. Jansen, E. A. Lomonova, A. J. A. Vandenput, and J. C. Compter, "Design tool for a 6-dof planar motor with moving permanent magnets and standstill coils," in *Proceedings of the 4^{th} international symposium on linear drives for industrial applications*, Birmingham, UK, Sep 2003, pp. 93–96.

[25] *Energy Calculations for Permanent Magnets, Engineering note AP062-9912.* Ansoft, 1999, pp. 1–3.

[26] A. B. J. Reece and T. W. Preston, *Finite element methods in electrical power engineering.* New York, USA: Oxford University Press Inc., 2000.

[27] *Flux3D 3.30 User's guide, volume 4: applications*, Cedrat, Meylan, France, Feb 2002.

[28] J. W. Jansen and C. M. M. van Lierop, "Contactless multi-dimensional planar actuator technology, iop-emvt 02204 a&b progress report," Eindhoven University of Technology, Tech. Rep., 2004, not published.

[29] H. D. Young and R. A. Freedman, *University physics*, 10th ed. Addison Wesley Longman, inc, 2000.

Appendix A

C++ code

A.1 Acceleration

```
// calculates the mass of the translator
//(assumes square magnets with halbach magnets) also sets the MCP
double masscalc(MagnetArrayDefinition *md, double back)
{
        double DensAlu = 2.7e3;
        double DensMag = 7.4e3;
        double MagnetMass, BackMass, area, mass;
        // # magnets X * # magnets Y *(size magnets^2+size magnets * size halbach * 2)
        // calc. for full array
        area = 49*(md->xdir[1]*md->xdir[1] + md->xdir[1]*md->ydir[1]*2);
        printf("area: %e\t height: %e\n", area, md->zdir[2]);
        MagnetMass = DensMag*md->zdir[2]*area;
        BackMass = DensAlu*back*area;   // neglects material above empty squares
        mass = MagnetMass + BackMass;
        // mass center point of translator
        md->mcp[2]=(MagnetMass*md->zdir[2]/2 + BackMass*(back+md->zdir[2]/2))/mass;
        printf("mcp: %f\n", md->mcp[2]);
        return mass;      // total mass in kg
}

void Motor::Accel(double mass, double f[], double Acc[])
{
        Acc[0]=f[0]/mass;
        Acc[1]=f[1]/mass;
        Acc[2]=(f[2]-9.81*mass)/mass ; // includes gravity
}
```

A.2 Optimizer

```
#include <vcl.h>
#pragma hdrstop
#include <iostream.h>
```

```
#include <math.h>
#include <algorithm>
#include <list>
#include "motor.cpp"
#include <stdio.h>
#define NPOINTS 15

//defines the magnets
void magnetdef(MagnetArrayDefinition *md, double hb)
{
   md->size[0]=7;
   md->size[1]=7;
   md->halbach=HALBACH;
   md->iron=IRONLESS;
   md->xdir[3]=md->ydir[3]=md->zdir[3]=1.17;
   md->zdir[0]=md->zdir[1]=md->xdir[1]=md->ydir[0]=20e-3;  // magnet side
   md->xdir[0]=md->ydir[1]=hb;                             // size halbach magnets
   md->xdir[2]=md->ydir[2]=md->zdir[2]=8e-3;               // magnet height
   md->mcp[0]=md->mcp[1]=0;
   md->mcp[2]=1.5e-3;
}

// defines the coils
void coildef
(CoilArrayDefinition *cd, double x, double y, double tau, double th, double h)
{

   cd->arraysize[0]=1;
   cd->arraysize[1]=1;
   cd->mcp[0]=x;
   cd->mcp[1]=y;
   cd->mcp[2]=-h/2;
   cd->turns=200;
   cd->xyspace[0]=cd->xyspace[1]=0;
   cd->size[0]=4*tau/sqrt(2)+th;                           //length (x)
   cd->size[1]=tau/sqrt(2)+th;                             //width  (y)
   if (cd->size[1] > (1.5*tau/sqrt(2)-0.5e-3))
           cd->size[1]=1.5*tau/sqrt(2)-0.5e-3;             //width  (y)

   cd->size[2]=h;                                          //heigth (z), 5e-3
   cd->size[3]=th;                                         //thickness
   cd->size[4]=cd->size[1]/2.0;                            //filet radius
}

void main (void)
{
   Motor *P = new Motor;
   MagnetArrayDefinition *md = new MagnetArrayDefinition;
   CoilArrayDefinition *cd = new CoilArrayDefinition;
   FILE *file[12];
```

```
int i, q,j,k;
double f[6];
double a[3];
double loc[6];
double HB[17];
double TH[17];
double current[2];        //number of coils
double x, y, tau, Ix, Iy, Iz, hb, back, mass, th, taun, h, Prel;
double Fx[NPOINTS+1], Fy[NPOINTS+1], Fz[NPOINTS+1];
double pos[3];

for (k=0; k<=16; k+=1)
     {
     TH[k]=6e-3+k*0.5e-3;
     printf("TH = %e\n", TH[k]);
     }

for (q=0; q<=16; q+=1)
     {
     printf("q = %i\n", q);
     HB[q]=5e-3+q*0.5e-3;
     printf("HB = %e\n", HB[q]);
     }

HB[0]=1e-3;

for(q=0;q<=16;q+=1)
{
     printf("q = %i\n", q);
     printf("HB = %e\n", HB[q]);
     printf("TH = %e\n", TH[q]);
}
// open data files
file[0]=fopen("cpp_x_accel.m", "a");
file[1]=fopen("cpp_y_accel.m", "a");
file[2]=fopen("cpp_Fx_accel.m", "a");
file[3]=fopen("cpp_Fy_accel.m", "a");
file[4]=fopen("cpp_Fz_accel.m", "a");
file[5]=fopen("cpp_Tx_accel.m", "a");
file[6]=fopen("cpp_Ty_accel.m", "a");
file[7]=fopen("cpp_Tz_accel.m", "a");
file[8]=fopen("cpp_Ax_accel.m", "a");
file[9]=fopen("cpp_Ay_accel.m", "a");
file[10]=fopen("cpp_Az_accel.m", "a");
file[11]=fopen("cpp_dat_accel.m", "a");
 for (i=0; i<12; i++)
   fprintf(file[i], "data=[");
q=0;
for (j=0; j<=15; j+=1)    // loop for conductor thickness
{
```

```
th=TH[j];

for (q=0; q<=14; q+=1)   // loop for halbach size
{
   h=7.7e-3;
   hb=HB[q]; // coil conductor height
   fprintf(file[11], "%.15e\t %.15e \n", th, hb);
   tau=20e-3+hb;        // tau = size magnets + size halbach
   back = 10e-3; //height of back material of translator
   magnetdef(md,hb);
   mass=masscalc(md,back); // calculates mass and also sets the MCP
   P->CreateMagnets(md);
   coildef(cd, 0, 0, tau, th, h); //2*tau/sqrt(2)
   P->CreateCoils(cd);
   coildef(cd, 0, 1.5*tau/sqrt(2), tau, th, h); //2*tau/sqrt(2)
   P->CreateCoils(cd);

   for (y=0; y<=tau/sqrt(2)+1e-10; y+=tau/sqrt(2)/25)
   {

      loc[0]=0;
      loc[1]=y;
      loc[2]=1e-3+md->mcp[2];// airgap + distance to MCP 6e-3;
      loc[3]=loc[4]=0;
      loc[5]=-M_PI_4; //Coils are shifted!!!!

      taun=tau/sqrt(2);

      //constant loss determination
      // reference point is Ix,z = 10 A @ h = 5 mm
      // Prelative = I^2/h => 20000 for ref => I can be calculated
      Prel=20000;
      Ix=Iz=sqrt(Prel*th);
      //end of cl
      current[0]=Ix*sin(M_PI*y/taun)+Iz*cos(M_PI*y/taun);
      current[1]=Ix*sin(M_PI*y/taun-1.5*M_PI)+Iz*cos(M_PI*y/taun-1.5*M_PI);

      P->Goto(loc);
      P->VisualDebug();

      //  P->Debug();
      P->Current(current);
      P->Force(2e-3, f);
      P->Accel(mass,f,a);
      fprintf(file[0], "%.15e ", loc[0]);
      fprintf(file[1], "%.15e ", loc[1]);
      for (i=2; i<8; i++)
         fprintf(file[i], "%.15e ", f[i-2]);

      for (i=8; i<11; i++)
```

```
            fprintf(file[i], "%.15e ", a[i-8]);

      }
      for (i=0; i<11; i++)
        fprintf(file[i], "\n");

      printf("%e\n", mass);

      P->Destroy();
   }
   }
   for (i=0; i<11; i++)
      fprintf(file[i], "];");
      fclose(file[i]);

   delete []md;
   delete []cd;
   }
```

Appendix B

Matlab code

B.1 RMS calculation

```
function out=rms(in)     % calculates the RMS value of the input vector values

n=length(in);            % returns the length of the vector

out=norm(in)/sqrt(n);    % 2-norm divided by no. of values = RMS value
```

B.2 Ripple calculation and plotting of the graphs

```
% This script calculates for every combination of TH and HB:
% - the mean value of the waveform
% - the percentual ripple of the waveform
% It also plots the results in mesh graphs

%load data
cpp_Az_accel
Az=data;
cpp_Ay_accel
Ay=data;

% initialize
th=0;
nx=0;
ny=0;

% calculates the mean value of the waveform for each combination of TH and HB
% y-direction (= x-direction with actuator)
for th=1:16
    nx=0;
    ny=ny+1;
    for hb=1:15
        nx=nx+1;
        outAy(nx,ny)=mean(Ay((th-1)*15+hb,:));
```

```
    end
end
% z-direction
th=0;
nx=0;
ny=0;
for th=1:16
    nx=0;
    ny=ny+1;
    for hb=1:15
        nx=nx+1;
        outAz(nx,ny)=mean(Az((th-1)*15+hb,:));
    end
end

% calculates the percentual ripple
% y-direction
ny=0;
for th=1:16
    nx=0;
    ny=ny+1;
    for hb=1:15
        nx=nx+1;
ripAy(nx,ny)=(rms(Ay((th-1)*15+hb,:)-mean(Ay((th-1)*15+hb,:)))
                                /mean(Ay((th-1)*15+hb,:)))*100;
    end
end
% z-direction
ny=0;
for th=1:16
    nx=0;
    ny=ny+1;
    for hb=1:15
        nx=nx+1;
        ripAz(nx,ny)=rms(Az((th-1)*15+hb,:)-mean(Az((th-1)*15+hb,:)))
                                            /mean(Az((th-1)*15+hb,:));
    end
end

% plot the figures
figure;
mesh(2e-3:0.7e-3:12.5e-3,1e-3:0.7e-3:10.8e-3, -outAy);
title('Acceleration in x-direction') % y in calculation, but x in report
xlabel('conductor bundle thickness TH (m)')
ylabel('side magnet size HB (m)')
zlabel('Acceleration (m/s2)');

figure;
mesh(2e-3:0.7e-3:12.5e-3,1e-3:0.7e-3:10.8e-3, -ripAy);
title('Acceleration ripple in x-direction')
```

```
xlabel('conductor bundle thickness TH (m)')
ylabel('side magnet size HB (m)')
zlabel('Percentual Acceleration ripple');

figure;
mesh(2e-3:0.7e-3:12.5e-3,1e-3:0.7e-3:10.8e-3, -outAz);
title('Acceleration in z-direction') % y in calculation, but x in report
xlabel('conductor bundle thickness TH (m)')
ylabel('side magnet size HB (m)')
zlabel('Acceleration (m/s2)');

figure;
mesh(2e-3:0.7e-3:12.5e-3,1e-3:0.7e-3:10.8e-3, -ripAz);
title('Acceleration ripple in z-direction')
xlabel('conductor bundle thickness TH (m)')
ylabel('side magnet size HB (m)')
zlabel('Percentual Acceleration ripple');
```

B.3 Corrections and filtering of the measured force

```
% filtering and correction for one force component
clear all;
close all;
load ms13;      % load measurement data
load mref3a;    % load reference measurements
load mref3b;

% correct for offset and baseline
baserest=ms13.Y(2).Data-(mref3a.Y(2).Data+mref3b.Y(2).Data)./2;
baserest=baserest-mean(baserest(5000:15000));

%filter, because the controller bandwidth is 50 Hz. Higher frequencies
%resulting from the movement of the bridge and the resonances
%of the translator are not suppressed.
[B,A]=butter(8,25/2500); % butterworth filter at 25 Hz. 2500 is sample freq/2
yf=filtfilt(B,A,baserest); % filter the signal (non-causal)
figure;
plot(ms13.Y(5).Data,yf,'k');

% plot result
grid on;
axis([-0.5 -0.1 -15 15]);
xlabel('position (m)','Fontsize',14);
ylabel('force F_x (N)','Fontsize',14);
```

Appendix C

Properties of the permanent magnetic material

The permanent magnets are supplied by Bakker Magnetics b.v., Son, The Netherlands. The magnet type is BM38SH, which is a grade of Neodymium Ferrite Boron rare-earth magnetic material. The magnets have a special rust protection and are therefore not coated. Figure C.1 and table C.1 show the properties of the material.

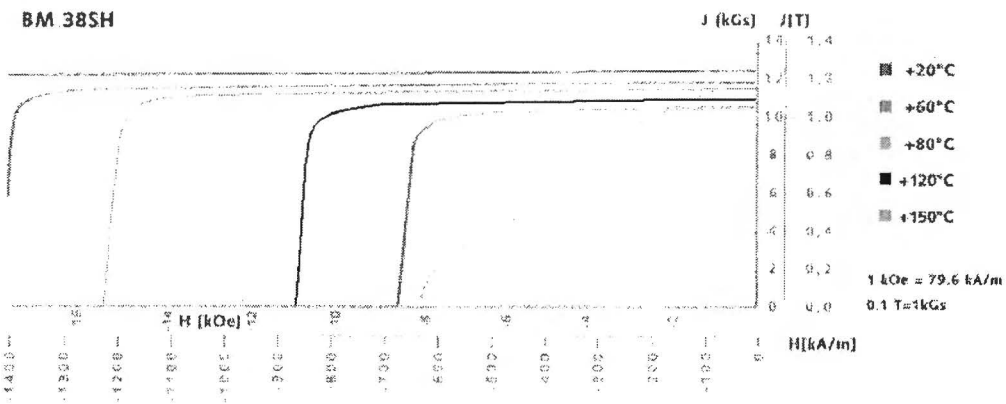

Figure C.1. *Properties of the BM38SH material*

	min	typical	dimension
Remanence B_r	1.20	1.24	T
Normal coercivity -HcB	890	950	kA/m
Intrinsic coercivity -HcJ		$\geq$ 1595	kA/m
max. energy product (B-H)max	287	302	kJ/m^3
Continuous max. operating temp.		160	^{o}C
Density		7.35	g/cm^3

Table C.1. *Properties of the BM38SH material*

Appendix D

Simulation results

D.1 FEM and C++ results for force calculation

Table D.1 to D.9 show the results of the force calculations by FEM and C++, for airgaps of 1, 2 and 3 mm. The current i in the coils is set according to equation 4.13, with $\hat{I}_x$ and $\hat{I}_z$ equal to 10 A. All results are based on two active coils.

Position (τ)	Calculated force (N) Lorentz (C++)	Lorentz(FEM)	Virtual Work (FEM)
-1.2500	-72.0950	-70.6732	-70.5028
-1.1944	-72.1164	-70.7016	-71.7588
-1.1389	-72.1822	-70.7812	-70.7828
-1.0833	-72.2865	-70.8982	-71.5340
-1.0278	-72.4613	-71.0763	-71.5454
-0.9722	-72.7095	-71.3180	-71.2188
-0.9167	-72.9614	-71.5581	-72.5166
-0.8611	-73.1307	-71.7150	-71.6566
-0.8056	-73.1922	-71.7704	-71.6777
-0.7500	-73.1639	-71.7436	-72.0224

Table D.1. *Force calculation F_x in FEM and C++ with 1 mm distance between magnets and coils*

D.2 Damping force due to eddy currents

Table D.10 shows the damping force that acts on the translator, due to eddy currents induced in the aluminium back plate, as a function of the thickness of the ceramic plate. The translator was moving at 2 m/s.

D.3 Induced eddy currents due to coil current

Table D.11 shows the eddy current power in the aluminium back plate of the model (see figure 4.12), as a function of the thickness of the ceramic plate. The current in

Position (τ)	Calculated force (N) Lorentz (C++)	Lorentz(FEM)	Virtual Work (FEM)
-1.2500	-0.0000	-0.0007	0.5774
-1.1944	0.0000	-0.0001	-0.2613
-1.1389	0.0000	0.0002	0.5986
-1.0833	-0.0000	-0.0008	0.4545
-1.0278	-0.0000	-0.0001	0.9560
-0.9722	-0.0000	-0.0010	-0.5638
-0.9167	0.0000	-0.0003	0.1786
-0.8611	-0.0000	0.0005	-0.5488
-0.8056	-0.0000	-0.0005	0.4075
-0.7500	0.0000	0.0003	-0.5919

Table D.2. *Force calculation F_y in FEM and C++ with 1 mm distance between magnets and coils*

Position (τ)	Calculated force (N) Lorentz (C++)	Lorentz(FEM)	Virtual Work (FEM)
-1.2500	71.3081	69.5468	69.8828
-1.1944	71.7831	70.0407	70.1766
-1.1389	72.2594	70.5286	70.1530
-1.0833	72.7420	71.0091	70.4490
-1.0278	73.2106	71.4753	71.2898
-0.9722	73.5940	71.8549	72.1417
-0.9167	73.8354	72.1082	71.3163
-0.8611	73.9571	72.2533	71.2080
-0.8056	74.0225	72.3496	72.0472
-0.7500	74.0641	72.4255	72.1609

Table D.3. *Force calculation F_z in FEM and C++ with 1 mm distance between magnets and coils*

the three coils is sinusoidal with a 90 degrees phase shift, with an amplitude of 3.5 A.

Position (τ)	Calculated force (N) Lorentz (C++)	Lorentz(FEM)	Virtual Work (FEM)
-1.2500	-66.9963	-65.6766	-65.2954
-1.1944	-66.9997	-65.6841	-66.1101
-1.1389	-67.0520	-65.7488	-66.8108
-1.0833	-67.1499	-65.8554	-66.4443
-1.0278	-67.3083	-66.0171	-65.7826
-0.9722	-67.5198	-66.2226	-65.8045
-0.9167	-67.7299	-66.4228	-67.5348
-0.8611	-67.8742	-66.5592	-67.0437
-0.8056	-67.9272	-66.6062	-66.9770
-0.7500	-67.8968	-66.5790	-66.8199

Table D.4. *Force calculation F_x in FEM and C++ with 2 mm distance between magnets and coils*

Position (τ)	Calculated force (N) Lorentz (C++)	Lorentz(FEM)	Virtual Work (FEM)
-1.2500	0.0000	-0.0005	0.4927
-1.1944	-0.0000	-0.0014	0.4630
-1.1389	-0.0000	0	0.3135
-1.0833	-0.0000	-0.0005	-0.3681
-1.0278	0.0000	-0.0000	-0.0898
-0.9722	0.0000	-0.0005	0.1455
-0.9167	-0.0000	-0.0004	0.7215
-0.8611	0.0000	0.0001	-0.1196
-0.8056	-0.0000	-0.0000	1.1213
-0.7500	-0.0000	-0.0004	0.2001

Table D.5. *Force calculation F_y in FEM and C++ with 2 mm distance between magnets and coils*

Position (τ)	Calculated force (N) Lorentz (C++)	Lorentz(FEM)	Virtual Work (FEM)
-1.2500	66.1839	64.5665	65.7613
-1.1944	66.6132	65.0112	65.9682
-1.1389	67.0579	65.4659	66.7330
-1.0833	67.5062	65.9141	67.2140
-1.0278	67.9314	66.3364	67.6656
-0.9722	68.2795	66.6853	68.1530
-0.9167	68.5110	66.9291	67.9560
-0.8611	68.6402	67.0786	67.9567
-0.8056	68.7134	67.1797	68.5092
-0.7500	68.7651	67.2628	68.0005

Table D.6. *Force calculation F_z in FEM and C++ with 2 mm distance between magnets and coils*

Position (τ)	Calculated force (N) Lorentz (C++)	Lorentz(FEM)	Virtual Work (FEM)
-1.2500	-62.2539	-61.0313	-60.6495
-1.1944	-62.2474	-61.0266	-61.3389
-1.1389	-62.2892	-61.0760	-61.0910
-1.0833	-62.3780	-61.1724	-62.0507
-1.0278	-62.5189	-61.3133	-61.2272
-0.9722	-62.6990	-61.4908	-61.4184
-0.9167	-62.8750	-61.6569	-61.7886
-0.8611	-62.9972	-61.7740	-61.8437
-0.8056	-63.0422	-61.8163	-61.6639
-0.7500	-63.0129	-61.7871	-60.6933

Table D.7. *Force calculation F_x in FEM and C++ with 3 mm distance between magnets and coils*

Position (τ)	Calculated force (N) Lorentz (C++)	Lorentz(FEM)	Virtual Work (FEM)
-1.2500	0.0000	-0.0014	0.7170
-1.1944	0.0000	-0.0012	-0.0335
-1.1389	0.0000	-0.0006	0.2690
-1.0833	-0.0000	0.0001	0.0485
-1.0278	0.0000	-0.0004	0.1802
-0.9722	0.0000	0.0003	-0.6726
-0.9167	0.0000	-0.0003	-0.2084
-0.8611	-0.0000	-0.0000	0.4218
-0.8056	-0.0000	-0.0001	0.0185
-0.7500	-0.0000	-0.0002	0.6578

Table D.8. *Force calculation F_y in FEM and C++ with 3 mm distance between magnets and coils*

Position (τ)	Calculated force (N) Lorentz (C++)	Lorentz(FEM)	Virtual Work (FEM)
-1.2500	61.4378	59.9477	61.8695
-1.1944	61.8247	60.3480	62.2034
-1.1389	62.2349	60.7684	61.7762
-1.0833	62.6480	61.1821	63.1141
-1.0278	63.0349	61.5659	63.7166
-0.9722	63.3532	61.8908	63.8845
-0.9167	63.5744	62.1247	64.2515
-0.8611	63.7081	62.2744	64.6095
-0.8056	63.7893	62.3812	64.2371
-0.7500	63.8506	62.4713	64.2960

Table D.9. *Force calculation F_z in FEM and C++ with 3 mm distance between magnets and coils*

Thickness of ceramic plate (mm)	damping force (N)
1	27.0
2.5	17.0
5	8.5
7.5	4.8
10	2.6
12.5	1.6
14	1.1

Table D.10. *Damping force on the translator due to eddy currents*

Thickness of ceramic plate (mm)	Power of induced eddy currents (W)
1	45.8
2	42.1
3	38.8
4	35.9
5	33.2
6	30.7
7	28.4
8	26.3
9	24.4
10	22.7

Table D.11. *Induced eddy currents due to current in the coils*

Appendix E

Pictures of the test setup

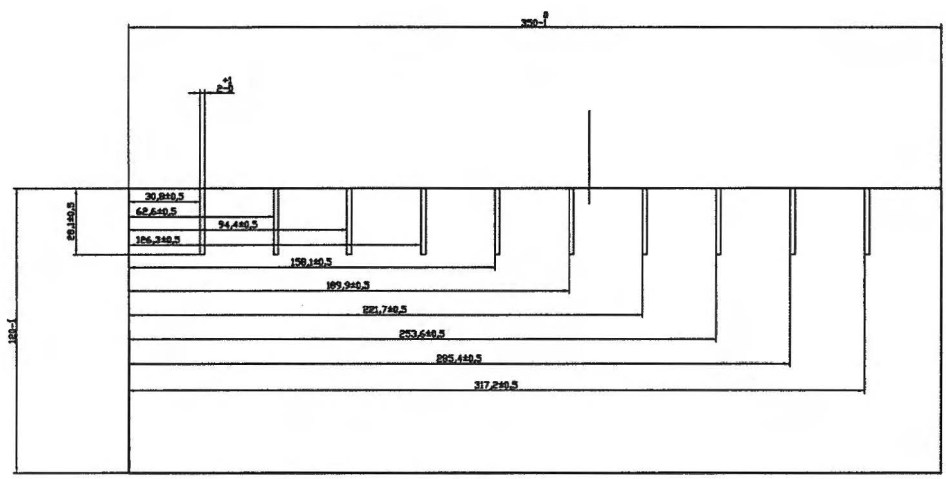

Figure E.1. *Technical drawing of the ceramic plate with grooves*

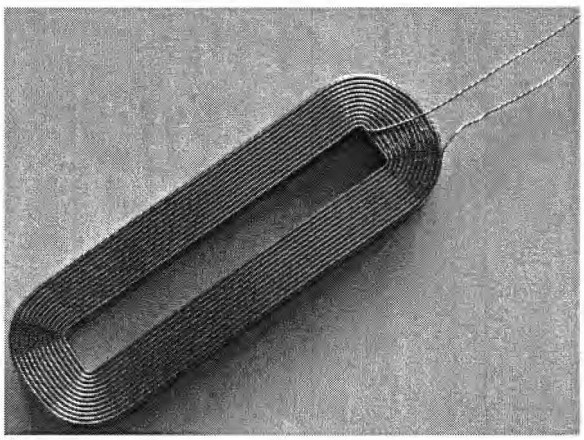

Figure E.2. *A coil*

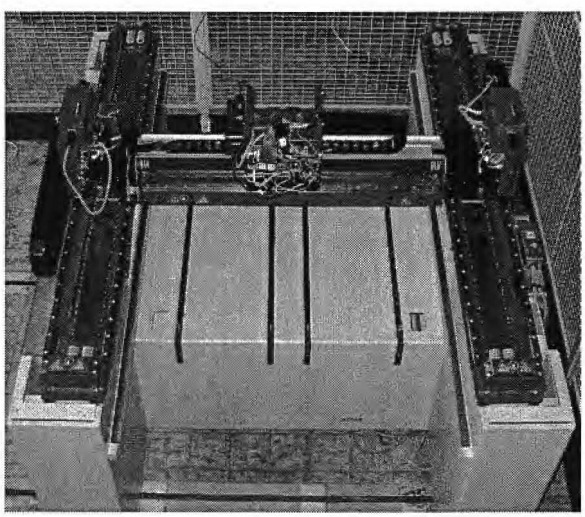

Figure E.3. *The H-drive in the lab*

Figure E.4. *The supporting construction for the stator of the 3-DoF actuator*

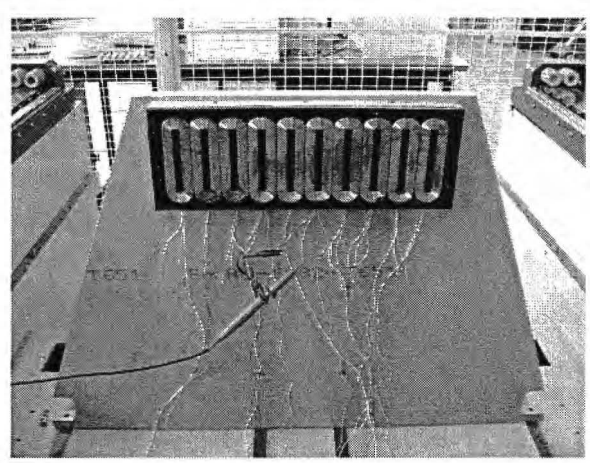

Figure E.5. *The stator placed on the support, ready for the EMF measurement*

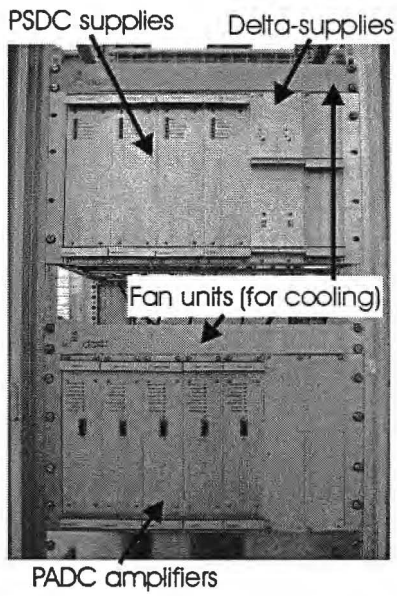

Figure E.6. *The power amplifiers and supplies in the 19" rack*

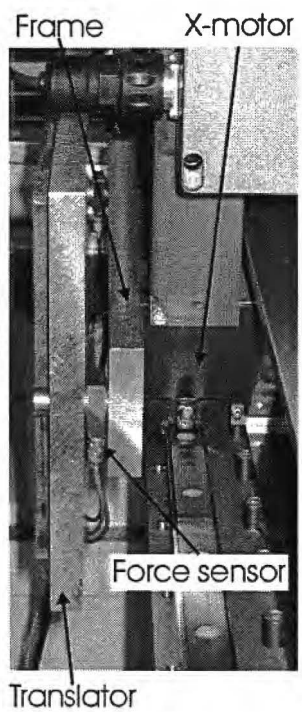

Figure E.7. *The translator, with force sensors, mounted to the* x*-motor*

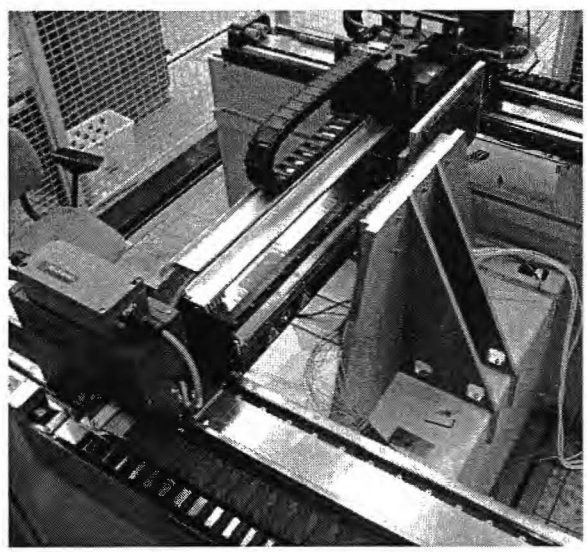

Figure E.8. *The total setup, ready for a quasi-static force measurement*

Appendix F

Measurement data

F.1 Coils

Coil no.	DC resistance (Ω)
1	6.25
2	6.26
3	6.24
4	6.23
5	6.25
6	6.24
7	6.23
8	6.23
9	6.23
10	6.28

Table F.1. *Resistance of stator coils*

Appendix G

Measurement equipment

G.1 H-drive

The H-drive is manufactured by Assembléon from Veldhoven. It is normally part of a pick and place system. Its accuracy is determined by the position sensors, that are mentioned in the next section.

G.2 Position encoders

The Heidenhain encoder rulers of the LIDA 201 type are the position sensors of the H-drive. These sensors have a micrometer (μm) accuracy. They are also used to determine the position of the 3-DoF actuator.

G.3 Force sensors

The force sensor, type Kistler 9251 A, can be seen in figure G.1. Its specifications are shown in table G.1. The sensors are connected to a charge amplifier. Its outputs are connected to the dSpace system. The amplifier is made by Hottinger Baldwin Messtechnik (HBM) and is a MGCplus AB22A.

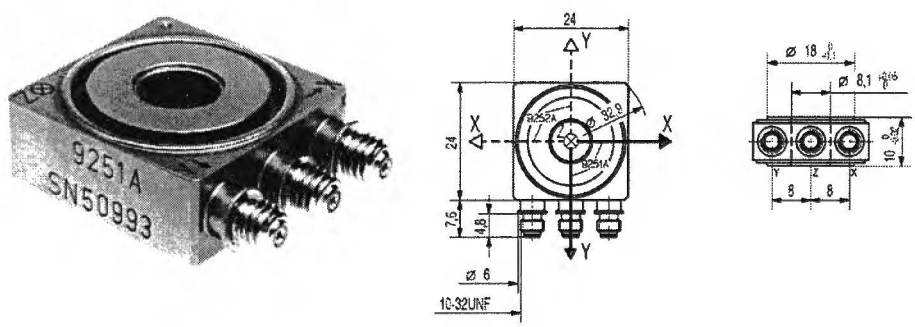

Figure G.1. *Force sensor with its dimensions*

Properties	value	unit
Range	-2,5 to 2,5	kN
Threshold	< 0.01	N
Sensitivity F_x, F_y	≈ -8	pC/N
Sensitivity F_z	≈ -4	pC/N
Cross talk F_x to F_z	$< 3\%$	
Cross talk F_z to F_x	$< 1\%$	
Rigidity c_x, c_y	1000	N/μm
Rigidity c_z	2600	N/μm
Operating temperature range	-60 to +150	°C

Table G.1. *Properties of the Kistler force sensor*

G.4 Temperature sensors

The temperature sensors are silicon temperature dependent resistors of type KTY 21-6. The properties of these sensors can be found in table G.2.

Properties	symbol	value	unit
Operating temperature range	T_{op}	-50 to +150	°C
resistance at 25 °C (min.)	R_{25min}	990	Ω
resistance at 25 °C (max.)	R_{25max}	1010	Ω
normal operating current	I_{op}	1	mA
max operating current	I_{opmax}	7	mA
max operating voltage	V_{opmax}	25	V
Package	-	TO-92 mini	-

Table G.2. *Properties of the KTY 21-6 temperature sensor*

The resistance of the sensor at a certain temperature can be calculated by using equation G.1:

$$R_T = R_{25} \times (1 + \alpha \times \Delta T_A + \beta \times \Delta T_A^2) \tag{G.1}$$

with $\alpha = 7.88 \cdot 10^{-3} K^{-1}$ and $\beta = 1.937 \cdot 10^{-5} K^{-2}$.

G.5 dSpace system

The dSpace system is used for the control of the H-drive and the power amplifiers of the 3-DoF actuator, as well as for recording the forces (from the force sensors), voltages and currents (from the power amplifiers). The system used is a modular board, which is extended with a sufficient number of digital I/O and analog I/O ports.

G.6 Scanner

The Agilent 34970 A Data Acquisition / Switch Unit is used for measuring the resistance of the coils by a four-wire measurement. Later, it is used as a scanner

to scan the resistances of the temperature sensors during tests. If the resistance of one of the sensors becomes too high, an alarm signal will be sent to the dSpace interface.

G.7 Measurement bridge

The measurement bridge that was used to measure the inductance of a single coil is made by Hewlett Packard. The type is HP 4194 A impedance / gain-phase analyser.